Rapid attribution of heavy rainfall events leading to the severe flooding in Western Europe during July 2021

Contributors

Frank Kreienkamp[1], Sjoukje Y. Philip[2], Jordis S. Tradowsky[1,4], Sarah F. Kew[2], Philip Lorenz[1], Julie Arrighi[7,8,9], Alexandre Belleflamme[16], Thomas Bettmann[18], Steven Caluwaerts[13,19], Steven C. Chan[14], Andrew Ciavarella[22], Lesley De Cruz[13], Hylke de Vries[2], Norbert Demuth[18], Andrew Ferrone[17], Erich M. Fischer[6], Hayley J. Fowler[14], Klaus Goergen[16], Dorothy Heinrich[7], Yvonne Henrichs[18], Geert Lenderink[2], Frank Kaspar[10], Enno Nilson[15], Friederike E L Otto[11], Francesco Ragone[13,20], Sonia I. Seneviratne[6], Roop K. Singh[7], Amalie Skålevåg, Piet Termonia[13,19], Lisa Thalheimer[11], Maarten van Aalst[7,8,21], Joris Van den Bergh[13], Hans Van de Vyver[13], Stéphane Vannitsem[13], Geert Jan van Oldenborgh[2,3], Bert Van Schaeybroeck[13], Robert Vautard[5], Demi Vonk[8], Niko Wanders[12]

1 - Deutscher Wetterdienst (DWD), Regionales Klimabüro Potsdam, Potsdam, Germany; 2 - Royal Netherlands Meteorological Institute (KNMI), De Bilt, The Netherlands; 3 - Atmospheric, Oceanic and Planetary Physics, University of Oxford, UK; 4 - Bodeker Scientific, Alexandra, New Zealand; 5 - Institut Pierre-Simon Laplace, CNRS, Paris, France; 6 - Institute for Atmospheric and Climate Science, Department of Environmental Systems Science, ETH Zurich, Zurich, Switzerland; 7 - Red Cross Red Crescent Climate Centre, The Hague, the Netherlands; 8 - Faculty of Geo-Information Science and Earth Observation (ITC), University of Twente, Enschede, the Netherlands; 9 - Global Disaster Preparedness Center, American Red Cross, Washington DC, USA; 10 - Deutscher Wetterdienst, Nationale Klimaüberwachung, Offenbach, Germany; 11 - School of Geography and the Environment, University of Oxford, UK; 12 - Department of Physical Geography, Faculty of Geosciences, Utrecht University, the Netherlands; 13 - Royal Meteorological Institute of Belgium, Brussels, Belgium; 14 - Newcastle University, Newcastle-upon-Tyne, UK; 15 - Federal Institute of Hydrology (BfG), Koblenz, Germany; 16 - Institute of Bio-and Geosciences (IBG-3, Agrosphere), Research Centre Jülich, Jülich, Germany; 17 - Administration of Technical Agricultural Services, Luxembourg, Luxembourg; 18 - Federal State Office for the Environment, Rhineland Palatinate, Germany; 19 - University of Ghent, Ghent, Belgium; 20 - Université Catholique de Louvain, Louvain-la-Neuve, Belgium; 21 - International Research Institute for Climate and Society, Columbia University, New York, USA; 22 - Met Office, UK

Main findings

- The severe flooding was caused by very heavy rainfall over a period of 1-2 days, wet conditions already before the event and local hydrological factors. While river discharge and water levels are the physical components most directly linked to the impacts of the event, we focus our assessment on the main meteorological driver, the heavy rainfall event. This is due to the fact that some hydrological monitoring systems were destroyed during the flood and data of sufficiently high quality and quantity is not currently available.

- The observed rainfall amounts in the Ahr/Erft and the Belgian part of the Meuse catchment broke historically observed rainfall records by large margins. In regions of that size the robust estimation of return values and the detection and attribution of trends is challenging and thus pushes the limits of what current methods of extreme event attribution are designed for.

- Therefore we broadened the analysis by assessing the influence of climate change on similar types of events that could occur anywhere in Western Europe in a large region between the north of the Alps and the Netherlands. We found that in the current climate, for a given location within this larger region, we can on average expect one such event every 400 years. That also means we expect such events to occur more frequently than once in 400 years within the larger Western European region.

- Climate change increased the intensity of the maximum 1-day rainfall event in the summer season in this large region by about 3 - 19% compared to a global climate 1.2 °C cooler than today. The increase is similar for the 2-day event.

- The likelihood of such an event to occur today compared to a 1.2 °C cooler climate has increased by a factor between 1.2 and 9 for the 1-day event in the large region. The increase is again similar for the 2-day event.

- These numbers are based on an assessment including observations, regional climate models and very high resolution climate models that directly simulate convection. The changes in intensity and likelihood are larger in the observation-based assessment compared to all models.

- In a climate 2 °C warmer than in preindustrial times models suggest that the intensity of a 1-day event would increase by a further 0.8-6% and the likelihood by a factor of 1.2-1.4. The increase is again similar for the 2-day event.

- The July 2021 floods resulted in extreme impacts including over two hundred deaths. Given the rarity of the event it is clear this is a very extreme event that is reasonably likely to cause negative impacts. However, especially given events like this will occur more frequently in the future, examining how vulnerability and exposure can be reduced becomes critical to reducing future impacts.

1 Introduction

The 6th Intergovernmental Panel on Climate Change (IPCC) assessment report (IPCC, 2021) states that extreme precipitation, pluvial and fluvial floods have been observed to increase in Western and Central Europe and will increase with high confidence in case global warming reaches 2 °C, expected to occur by mid-century in case greenhouse gas emissions reduction do not take place quickly. However, attribution of specific local extreme precipitation events to climate change remains difficult due to the high year-to-year or decade-to-decade variability of extreme precipitation. Furthermore, the limited availability of finely-resolved climate model simulations and long-term observations provides challenges to attribution studies of local-scale events.

Extreme rainfall occurred in Germany, Belgium, Luxembourg and neighbouring countries during the period 12 to 15 July 2021, leading to severe flooding particularly in North Rhine-Westphalia and Rhineland-Palatinate in Germany and along the river Meuse and some of its tributaries in Belgium and the Netherlands. The flooding resulted in at least 184 fatalities in Germany[1] and 38 in Belgium[2] and considerable damage to infrastructure, including houses, roads, communication, motorways and railway lines as well as bridges. A variety of livelihoods were severely disrupted by the flood event, including local businesses in the affected regions and wine growers that make up the backbone of the Ahr Valley region (Tafel and Szolnoki, 2020). Road closures left some places inaccessible for days, cutting off some villages from evacuation routes and other forms of emergency response. The most affected areas are around the rivers Ahr and Erft as well as the Vesdre in the basin of the Meuse. An estimate by the German Insurance Association (GDV) describes the cost of the event at €4.5 to €5.5 billion for Germany alone while damage in Belgium is estimated to exceed €0.35 billion[2]. The devastating impacts of the July 2021 extreme precipitation event that struck Germany and Benelux provides an impetus to carry out an event attribution analysis to investigate the role of anthropogenic climate change in the extreme rainfall event. This analysis follows the standard structure of WWA event attribution analysis (van Oldenborgh, et al. 2021) by defining the event, describing data and models used, assessing trends, attributing the event, synthesis of the results which are put in the context of vulnerability and exposure.

1.1 Meteorological Situation

The extreme precipitation occurred in connection with the slowly-moving low-pressure system "Bernd"[3]. As reported by DWD (Junghänel et al., 2021), MeteoLux[4] and RMI[5], the meteorological situation during the 12 to 15 July period was mainly characterised by a cut-off low pressure system over Central Europe (Figure 1), supplying very moist air to the wider region, see Figure 2. In conjunction with the low pressure system slowly approaching from France towards Germany, the troposphere was increasingly unstably stratified. Surface air over the Mediterranean and Northern Europe was very

---

[1] EM-Dat, 10.08.2021, https://public.emdat.be/data (retrieved 10 August 2021)

[2] Crisiscenter Belgium, 19.09.2021.

[3] The naming of the low and high pressure systems here follows the German naming convention. Information on this can be found under http://www.met.fu-berlin.de/adopt-a-vortex/ .

[4] MeteoLux, 19.07.2021, https://www.meteolux.lu/de/aktuelles/ruckblick-auf-den-ergiebigen-dauerregen-vom-14-und-15-juli-2021/?lang=fr

[5] RMI, 16.07.2021 , https://www.meteo.be/nl/info/nieuwsoverzicht/eerste-cijfers-en-duiding-bij-de-hevige-neerslag-van-14-en-15-juli (Dutch) and https://www.meteo.be/fr/infos/actualite/ce-que-lon-sait-sur-les-pluies-exceptionnelles-des-14-et-15-juillet-2021 (French)

warm, feeding the atmosphere's water holding capacity. Warm, and very humid, air masses reached Central Europe from the Mediterranean in a rotating movement around the low pressure system "Bernd". Forced uplift (orographic and dynamic) and slight damming effects in the western low mountain ranges (Ardennes, Sauerland, Westerwald and Eifel) then led to recurrent or persistent heavy rain, first regionally and later over large areas. This initially led to localised overflow of small watercourses and flash floods. As the precipitation continued, medium-sized and larger rivers such as (in Germany) the Ahr, Emscher, Erft, Kyll, Lippe, Prüm, Ruhr, Rur, Sieg and Wupper also overflowed their banks. This resulted in an extensive flood situation from the Eifel (Rhineland-Palatinate) through the Rhineland and the Ruhr region to southern Westphalia (North Rhine-Westphalia). In Belgium, the worst floods occurred in the Ardennes along the Vesdre and Ourthe rivers and then downstream along the Meuse. In the days after 15 July, the high pressure system "Dana" pushed the low pressure system "Bernd" towards south-eastern Europe. This again led to further heavy rainfall events in Germany (Eastern Erzgebirge and Lausitz, as well as in the Berchtesgadener Land, 17 July 2021).
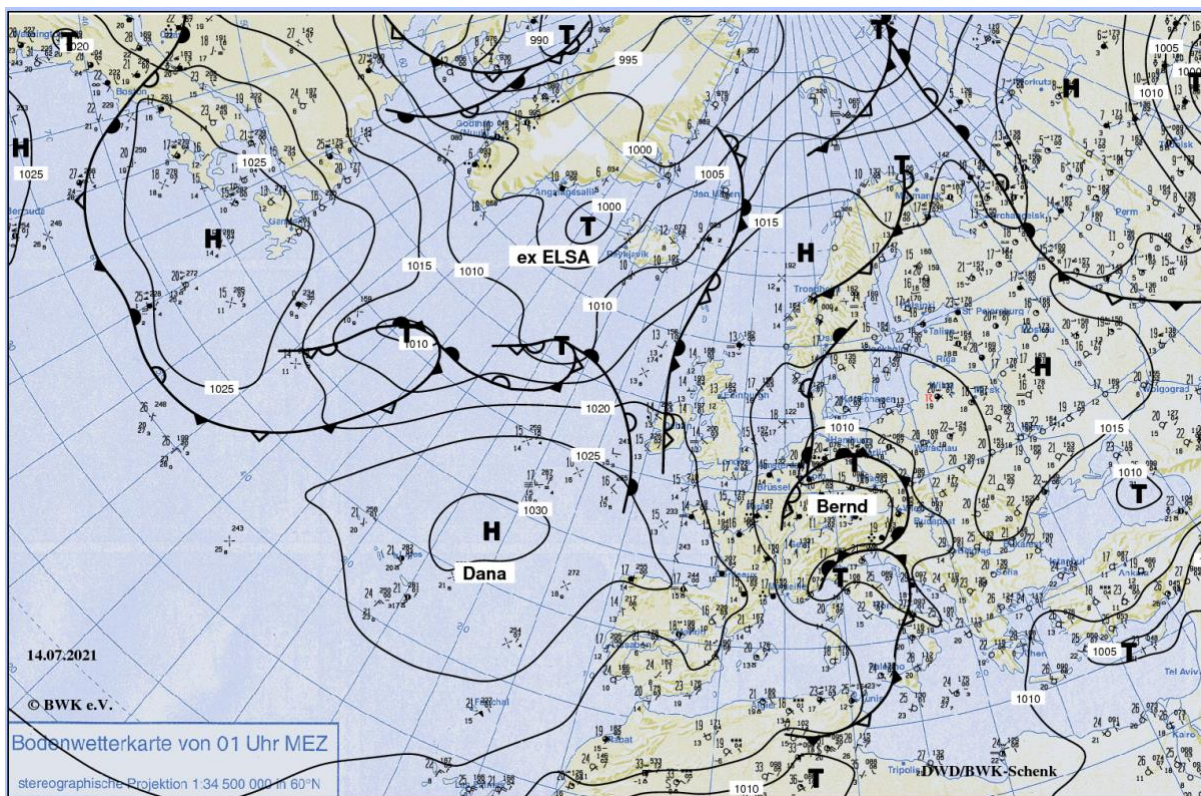
Figure 1: Analysis of the meteorological situation on 14 July 2021 0 UTC. The rights for the illustration are held by Berliner Wetterkarte e.V. (https://berliner-wetterkarte.de/)
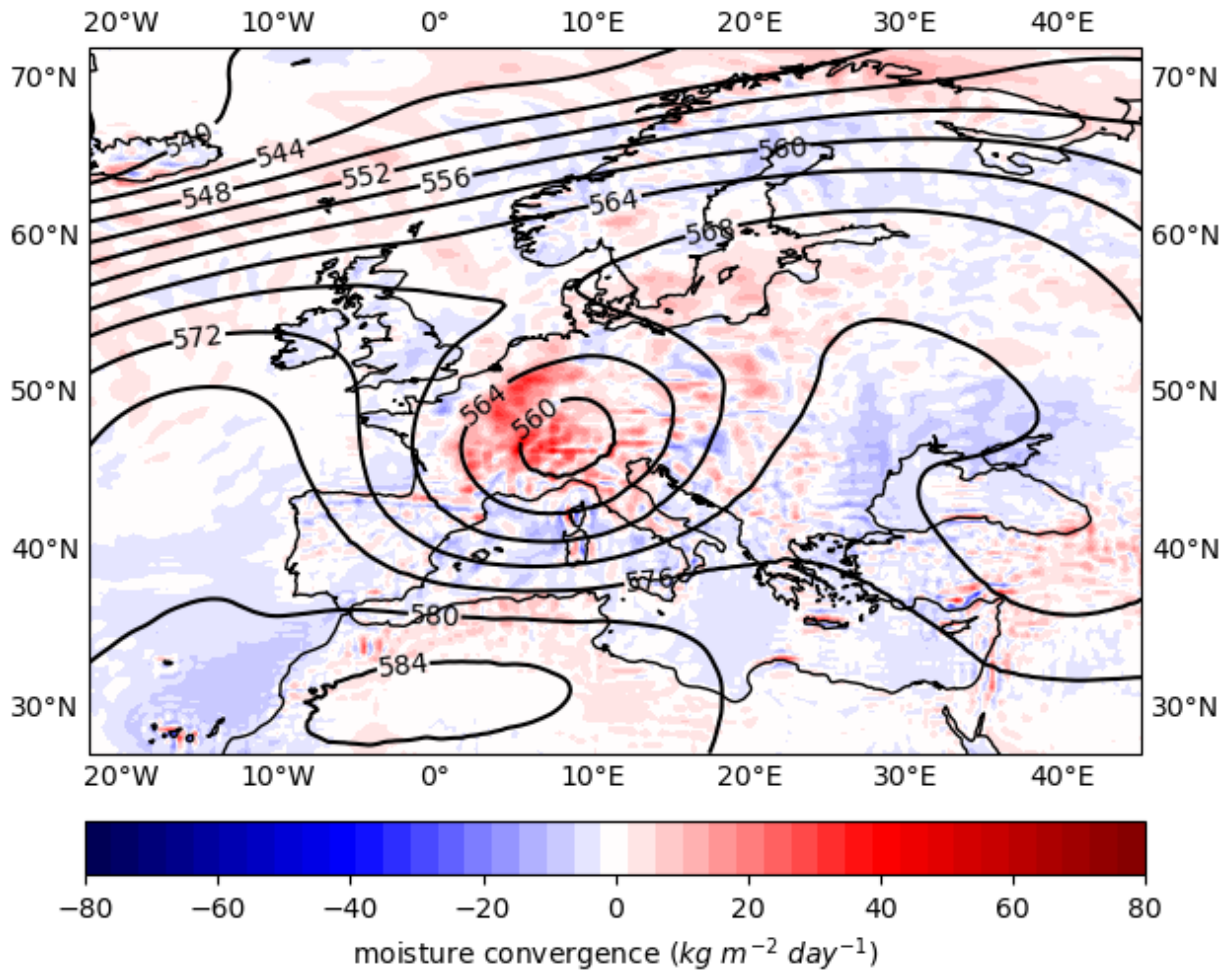
Figure 2: Meteorological situation during the event. Contour lines show the 500 hPa geopotential averaged over the 12-15 July 2021 period (in 10^2 m^2 s^{-2}). Colors show the vertical integral of the convergence of moisture flux, averaged over the 12-15 July 2021 period (in kg m^{-2} day^{-1}). Data from the ERA5 reanalysis. The data show a nearly stationary cut-off low over central Europe, associated with moisture convergence over the region and divergence over the Mediterranean region and the Atlantic ocean south 40° N.

In addition to the amount of precipitation, the antecedent soil moisture content is also relevant in the context of flooding. The three weeks before the flood event were marked by recurring precipitation events throughout a broader Western Europe region including both affected regions in Germany and Belgium (overall moderately wet conditions over the Belgian Meuse basin in the month before). The soils were therefore already near saturation in some parts of the area affected by heavy rainfall associated with low-pressure system "Bernd" (see Figure 2 in Junghänel et al., 2021). While in Rhineland-Palatinate and in South Westphalia the soils could hardly absorb any additional water regionally (in some cases they had less than 10 mm free soil water storage), the soils in the south-west of North Rhine-Westphalia were still capable of absorbing water to a certain extent (over 75 mm free soil water storage).

1.2 Hydrological analysis

This section provides background on the hydrological setting of the affected areas and attempts to provide first estimates of the hydrological extremes associated with the extreme hydrometeorological conditions and thereby also linking the first-order drivers (rainfall) with their effects (flooding). Special focus is put on the Meuse (gauge Eijsden, middle Meuse) and the Ahr (gauge Altenahr, lower Ahr). Due to limited high-quality data availability and decreased reliability as well as complexity of hydrological drivers, a full hydrological attribution study is considered not possible at this point for the hydrological time series.

1.2.1 Hydrological characteristics of the affected areas

The affected catchments selected for this study (see metadata Table 1 and Figure 5) are located in the Ardennes and the Eifel mountains in the north-western part of the Central European low mountain range. This region is geologically characterised by paleozoic siliciclastic sedimentary rocks, regionally also limestones, locally interbedded with paleogene and neogene volcanic rocks. Relatively shallow soils have often developed on these siliceous rocks. They have a low water capacity also due to their high skeletal content. Topographically, it is an elevated plain (mostly 200 to 500 m) surmounted by individual mountain ranges (up to 700 m), into which the river network has cut deeply during an ongoing phase of tectonic uplift, often in the form of V-shaped notch valleys. The valleys are locally very narrow with steep slopes leading to funnel-like effects in the event of floods.

These hydrogeological, pedological, and topographical characteristics pre-condition the area to be prone to an overall high and rapid hydrological responsiveness. In combination with the extreme hydro-meteorological situation in July 2021, characterized by high soil saturation levels, low saturated conductivity and high and sustained precipitation intensities over a widespread area set the scene for the extreme and destructive hydrological event.

It should be noted that the winter is the usual flood season, i.e. the time of the highest annual discharge, in the region, when relatively high precipitation, low evapotranspiration, possibly in combination with snowmelt, cause high discharges. Nevertheless, many large floods caused by heavy rainfall have occurred in past summers, e.g. 1804, 1888, 1910, 2016 in the Ahr region (Roggenkamp & Herget, 2014).

In addition to many common features of the catchments, there are also differentiating characteristics that have a modifying effect on the flood. At the level of the various catchments, in addition to the location relative to the precipitation area and regional hydrological, topographical and pedological details, different land cover (arable and grassland use, degree of forestation, viticulture) and water management measures (dams, flood retention) should be mentioned. At the level of the individual rivers, the respective valley cross-sections, river construction, building development near the river and effects during the event itself (backwater, surges) cause large differences in the local flooding.

Figure 3 shows hydrographs of selected gauging stations during the event period. The catchments of the Vesdre, Ahr, and Kyll responded particularly fast. At all gauging stations pre-existing water level maxima (red lines in Figure 3) were significantly overtopped, including the station Eijsden at the relatively large basin of the Meuse. For Belgium (Meuse catchment) out of the 118 stations where discharge is measured, the discharge exceeded the threshold corresponding to the 25 year return period in more than half of the locations, and the threshold corresponding to the 100 year return period was exceeded in 29 locations. Additionally, preliminary reporting indicates that, out of the 262 Walloon communities, 197 received excessive rainfall.

Table 1 gives some general statistics and data sources for the stations. Locations can be found in Figure 4.
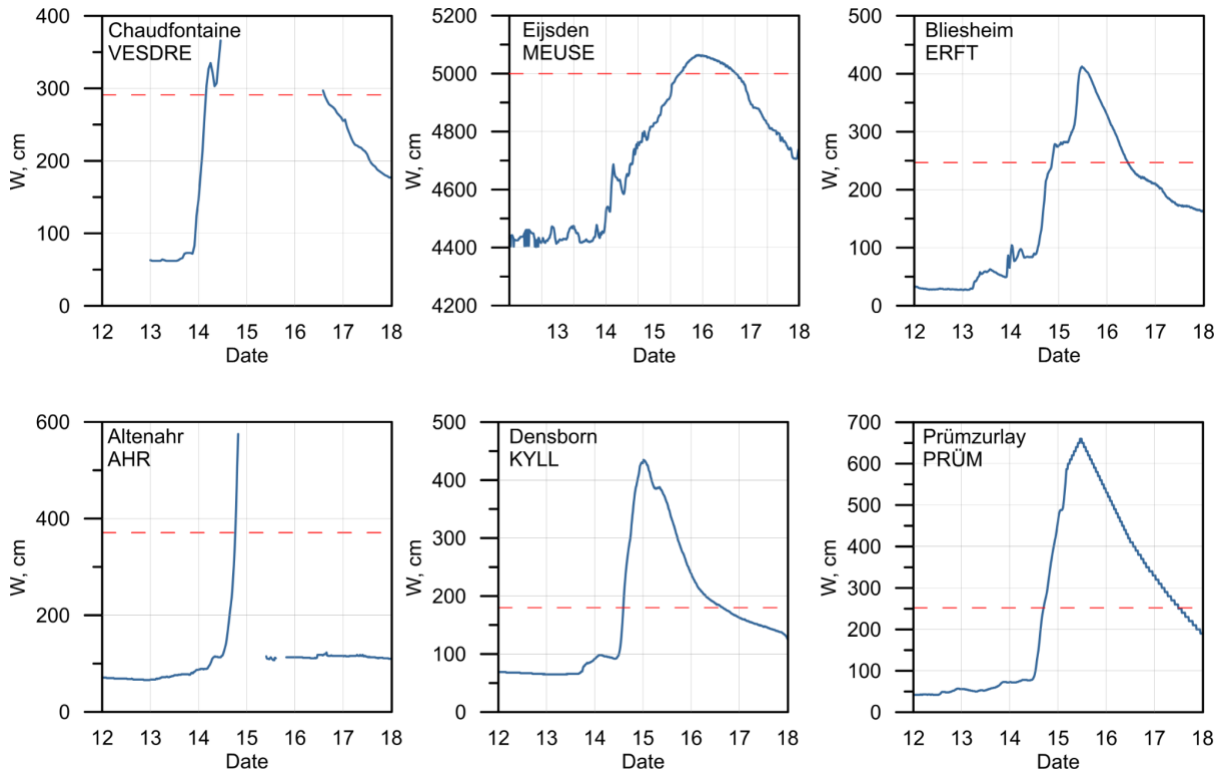
Figure 3: Water levels between 12 and 18 July 2021 at selected gauging stations. Red hatched line shows the highest observed water levels according to pre-July 2021 hydrological statistics (except for Eijsden/NL showing a "extreme" scenario). Plot: Federal Institute of Hydrology (BfG). Sources: Table 1.

Figure 4: Map of the catchments and locations of gauging stations.

Table 1: Selected catchment areas, gauging stations and hydrological parameters. MQ (mean discharge), MHQ (mean of highest annual discharge), HHQ (highest observed discharge), HQ100 (statistical discharge with return period of 100 years). Sources: DGJ (Deutsches Gewässerkundliches Jahrbuch), LfU RLP (Federal State Office for the Environment, Rhineland Palatinate), LANUV (Federal State Office for Nature, Environment and Consumer Protection), RWS (Rijkswaterstaat, the Netherlands), SPW-MI (Service Publique de Wallonie - Mobilité et Infrastructures, Belgium).

River	Gauging station	Catchment area (at gauging station) [km²]	Time period (quality checked data)	MQ [m³ s⁻¹]	MHQ [m³ s⁻¹]	HHQ (before July 2021) [m³ s⁻¹]	HQ100 [m³ s⁻¹]	Source
Ahr	Altenahr (DE)	746	1946 - 2019	6,86	90,3	236	241	DGJ, LfU RLP
Kyll	Densborn (DE)	472	1973 - 2019	6,7	89,5	180	190	DGJ, LfU RLP
Prüm	Prümzurlay (DE)	574	1973 - 2019	7,78	110	252	278	DGJ, LfU RLP
Erft	Bliesheim (DE)	604	1964 - 2020	2,47	26,48	55,8	71	DGJ, LANUV
Vesdre	Chaudfontaine (BE)	683	1992 - 2020	10.63	119.3	274.5		SPW-MI
Meuse	Eijsden (NL)	~20500	1911 - 2021	255	1473	3050	2779	RWS

1.2.2 Hydrological data availability

A precise reconstruction and classification of the hydrological and hydrodynamic processes of 14 and 15 July 2021 will require additional surveys because in many places the extreme floods not only far exceeded any previous event but also led to a failure or even destruction of the gauging stations. Therefore, only sparse water-level measurements are available for some catchments (e.g. Ahr, Vesdre). Instead of water level data, discharge data would be more suitable to describe the hydrological phenomenon and to evaluate the 2021 event against the background of long term measurements. However, existing discharge values can also only be used to a limited extent. Even if water level data has been recorded, existing water level-discharge relationships in most cases do not cover the extremely high water levels of the July 2021 event and/or the event has strongly changed the water level-discharge relationships due to considerable morphological effects in the valleys and river beds. An enormous transport of sediment and suspended matter has not only changed the properties of the water but is not accounted for in the existing water level-discharge relationships. Especially the entrainment of large amounts of sediment and flotsam led to shifts in the discharge cross-section and to pulsating backwater and surge processes in the watercourse. These non-stationary hydraulic processes cause major difficulties in plausibility checks of measured sediment lines or the reconstruction of discharges.

For the current rapid assessment, it is therefore necessary to rely on the available preliminary and relatively uncertain observational data, initial estimates based on individual water level marks or indirect methods such as hydrological models or a balance based on neighbouring gauges of larger rivers. Table 2 provides an overview of the currently available data sources and discharge estimates for the middle Meuse and lower Ahr.

Table 2: Overview of preliminary data for a peak flow ($m^3 s^{-1}$) reconstruction in selected catchments at the time of compilation and unpublished approximate peak flow values.

River	Method	Temporal (spatial) resolution	Q-Peak (m3/s)	Remarks	Source
Ahr	Observation Altenahr	15 Min.	555	Raw data, based on last measurement and extrapolated water level-discharge relationships low estimate	Federal State Office for the Environment, Rhineland Palatinate (LfU RLP)
Ahr	Hydrological Model HBV, Altenahr	1 h (lumped)	565,37	Update run of a forecasting model for the Rhine River (not optimised for the Ahr) low estimate	Federal Institute of Hydrology (BfG)
Ahr	Local flood mark in Walporzheim (4 km upstream of Altenahr)	none (peak)	1300 1200	high estimate low estimate	University of Bonn; Roggenkamp & Herget (pers. comm.)
Ahr	Local flood mark in Dernau (6 km upstream of Altenahr)	none (peak)	1200 1000	high estimate low estimate	University of Bonn; Roggenkamp & Herget (pers. comm,)
Ahr	Hydraulic model SOBEK Rhein based on measurements at Andernach and Bonn	15 min	1250	Indirect information based on Rhine gauges (raw data)	Federal Institute of hydrology (BfG)
Ahr	Hydrological model ParFlow, Altenahr	1 h	1191	Uncalibrated, physically based, integrated hydrology model	Research Centre Jülich (FZJ), Kollet & Maxwell (2006, 2008), Kuffour et al. (2020)
Ahr	Estimate based on shift and subtraction of time series at Bonn (-3h) and Andernach (+ 3h)	15 min	1130	Rough estimate based on raw data	Federal Institute of Hydrology (BfG)
Meuse/Maas	Gauging data Eijsden	10 min/daily	3179	Gauging data	Rijkswaterstaat (RWS)

1.2.3 Estimation of peak flows

Based on the available data, we choose two gauging stations and two different hydrological settings for further estimation of peak flows and return periods: Altenar (lower Ahr, fast reacting relatively small catchment), and Eijsden (middle Meuse, slower reacting larger catchment).

1.2.3.1 Meuse (Eijsden)

- Peak flow: 3179 $m^3 s^{-1}$; 15 July 2021 (17:30)
- Day mean: 2794 $m^3 s^{-1}$; 15 July 2021

The currently available data have to be regarded as raw data which did not pass all necessary quality checks. For example, Figure 3 shows some noise in the data of gauge Eijsden/Meuse which may be reduced in the final time series. Nevertheless, under the given conditions, the data situation at larger rivers such as the Meuse can be regarded as good. Especially since no overbank flooding occurred and thus the discharge-water level relationship is still reliable.

The Eijsden gauging station offers a continuous and long time series at a daily temporal resolution. These data, as well as the peak flows, can be directly interpreted. The peak flow of the Meuse at the border between Belgium and the Netherlands is estimated as 3179 m^3 s^{-1} (15 July 2021, 17:30). The highest daily mean discharge was 2794 m^3 s^{-1} (15 July 2021).

High water levels in the Meuse normally occur in the winter period when the upstream catchment is fully saturated due to prolonged rain periods or rain-on-snow runoff events. The flood on 15 July 2021 is exceptional as it was the highest on record summer flood event. Previous events in summer never exceeded 2016 m^3 s^{-1} (22 July 1980), putting 2021 outside of the expected flood volumes based on the historic summer floods records for the Meuse with a 40% increase compared to the previous summer flood record.

Water management interventions, like intentional flooding of wetlands, prevented downstream floods and kept the Meuse river within its banks. However, it must be noted that the current flood levels were equal to the design levels (return period 1 in 250 years) of the major dike systems that were put in place after the winter floods of 1993 and 1995. These adaptation measures prevented the widespread flooding of the river Meuse during this event.

1.2.3.2 Ahr (~Altenahr, lower Ahr)

- Ahr peak flow: 1000 m^3 s^{-1} (+/- 200 m^3 s^{-1}); 15 July 2021 (03:00)
- Ahr day mean: 600 m^3 s^{-1} (+/-50 m^3 s^{-1}); 15 July 2021

Compared to the Meuse, the data situation is much more complicated for the Ahr as measurements are fragmentary. High-resolution measured data (up to 15 minutes) from the Ahr are available e.g. from gauging station Ahrweiler until 14 July 2021, 19:45:00 only, the time the station was destroyed. At this time discharge was 555 m^3 s^{-1} (LfU RLP). The peak flow occured early on 15 July 2021 and must have been much higher. First peak flow estimates based on local water level surveys in connection with preliminary cross-section surveys (Univ. Bonn, Dr. Thomas Roggenkamp, pers. comm.) point to flows higher than 1200 m^3 s^{-1} (Walporzheim) and higher than 1000 m^3 s^{-1} (Dernau), 4 km and 6 km upstream, respectively. A peak flow higher than 1100 m^3 s^{-1} is consistent with estimates from gauging stations at the Rhine (Andernach, Bonn) flanking the mouth of the Ahr river. These estimates account for the volumes and wave travel times in this section of the Rhine (Duong et al., 2021). Furthermore, hydrological model outputs - simulations driven by observed meteorological data of the event - were taken into account. It must be noted however, that due to simplifications, these models are not optimised to simulate extreme situations in small rivers such as the July 2021 event. For example, wave routing routines are not able to account for flooding effects such as backwater at bridges and other bottlenecks or surges following infrastructure breakdown. Nevertheless, accounting for hydrological aspects of the event (precipitation, pre-conditions on the ground) modelled data give a range of about 600 to 1200 m^3 s^{-1}.

In this preliminary multi-evidence reconstruction we give high weight to the results of water level / cross section surveys and the estimates based on continuous observations on the Rhine river. This leads us to a rough estimate of peak flow of the Ahr in the order of 1000 m^3 s^{-1} (+/- 200 m^3 s^{-1}) which must have occurred early on 15 July 2021 (03:00). For this day, mean discharge is estimated to 600 m^3 s^{-1}

(+/-50 m^3 s^{-1}) based on the routed difference of gauging stations Andernach and Bonn (Rhine) shifted to the timing of the wave at Ahrweiler (Ahr).

The estimated peak flow of 1000 m^3 s^{-1} (+/-200 m^3 s^{-1}) was by a factor 4.2 (3.4 to 5.0) higher than the highest peak on record since 1947 before the event (236 m^3 s^{-1}, June 2, 2016). It is almost as high as the highest peak flow documented and quantified so far (summer 1804, about 1200 m^3 s^{-1} in Walporzheim, 4 km upstream of Altenahr; Roggenkamp & Herget, 2014, 2015). Preliminary estimations of the return period for the hydrological event by the Federal State Office for the Environment Rhineland Palatinate (LfU RLP) lead to values of 1 in more than 500 years for the July 2021 event. For this analysis, the sample of peak values since 1947 was extended by the event 2021 and historical events of 1804, 1888, 1910, 1918, and 1920 as documented by Roggenkamp & Herget (2014).

The estimated daily mean of 600 m^3 s^{-1} (+/-50 m^3 s^{-1}) on Jul 15 was by a factor 3.7 (3.4 to 4.0) higher than the highest daily mean observed before (162 m^3 s^{-1} on 21 December 1993). A first rough approximation of the return period of the daily mean including the recorded HQ values (daily means since 1947) leads to a return period 1 in more than 500 years. Historical flood marks can not be used here because they are not conclusive for daily mean flows.

1.2.4 Conclusions and Discussion of the hydrological analysis

The July 2021 flood in the regions investigated (lower Ahr and middle Meuse) here
- a) Was significantly higher than any flood since the beginning of systematic records.
- b) Overtopped not only the records but also the extreme values HQ100 and higher determined from the recorded data.
- c) Is in some catchments comparable only to the highest historically documented and quantified events (Ahr).
- d) Has an initial and very uncertain estimated return period of 1 in more than 500 years (Ahr) for the hydrological event.

Although some first estimates could be given on the hydrological characteristics of the event, the data situation is very poor. Evaluating floods over long periods of time (as necessary for a hydrological attribution study) is hampered by the overall complexity and heterogeneity of flood-generating processes in the Eifel/Ardennes region, given the topographic and hydrogeologic properties of the catchments and water management measures (e.g. Karst in the upper Meuse, reservoirs in some Meuse tributaries, fast reacting topographic/hydrogeological settings of the Ahr). Annual flow maxima usually occurs during the winter season. Summer events have occured and have been destructive but were relatively rare in pluvial flow regimes of central Europe. Also the pre-conditions (at least weeks before the event) play a significant role.

In the Eifel region, annual highest river flows (MHQ) have increased by to +8 to +10% from the 1950's until today (based on observations; Nilson & Iber, 2021). Future changes amount to about +10% (ensemble median, ensemble range +5% to +20%, based on RCP8.5), mostly due to winter floods.

Overall, attribution of changes in extreme river flood occurrence is hampered by several factors, including the contribution of local surface characteristics as well as human water management. These issues are also noted in the recent IPCC 2021 report (Chapter 11: Seneviratne et al., in press), which assesses that regional changes in river floods are more uncertain than changes in pluvial floods because complex hydrological processes and forcings, including land cover change and human water management, are involved. Adding to the overall uncertainties associated with the discharge data of the event and the simulation data, the sample of data is too small to allow an appropriate determination of

the return periods for rare and extreme events such as the flood of July 2021. Statistical weather generators and simulations with improved hydrological models could be used to obtain better estimates. Due to all these aspects and effects, focussing on hydrological phenomena (floods, discharge) seems not to be a good choice for this attribution study. We therefore focus the attribution study presented in the following chapters on the meteorological phenomena, i.e. heavy precipitation accumulated over the course of one and two days.

1.3 Analyzed Regions

While the extreme precipitation in Germany and Belgium was embedded into the same large-scale precipitation system, the characteristic differed between the regions and thus we have decided to analyse several regions (see Figure 5) with impact-relevant meteorological indices characterizing the event. In addition to hydrological differences between the affected catchments, the regions we analyse in this study also differ in their spatial extent.

In this study, we (1) consider two severely impacted catchment-shaped regions for which we ask the attribution question of how much climate change made the event more intense or more probable, and (2) also address a more general question of how much climate change altered the probability and intensity of similar events to occur anywhere in Western/Central Europe (from north of the Alps to the Netherlands), an area characterised by precipitation climatologies similar to those in the regions affected by flooding in July 2021.

The regions which we are analysing in the following are:
- Ahr/Erft; combined black polygons in Figure 5: A region that covers the catchment areas of the Ahr and Erft. Since we did not have a shape file of the Ahr-Erft catchments at the beginning, we used a simple polygon shape, which describes the region very roughly, for the analysis of observational data and model simulations.
- Belgian Meuse catchment upstream of Eijsden; red polygon in Figure 5.
- "Pooling Region" (covering the region north of the Alps to the Netherlands); we considered the event as the occurrence of an extreme precipitation event in any of the 14 blue tiles in Figure 5. This has the advantage of increasing the amount of data available for the statistical evaluation of the event, and enables us to study more generally extreme precipitation at the larger scale (130 km) in a region from north of the Alps to the Netherlands. For this approach we pool 14 non-overlapping rectangular tiles of dimension 130 km x 130 km. The 14 rectangular regional tiles were carefully selected after checking the mean and extreme precipitation statistics (parameters of the GEV fitted distribution) to make sure that the set was homogeneous and can be considered as belonging to the same statistical population.

The severe flooding in the Ahr and Erft region was caused by a short intensive precipitation period, i.e. most of the rainfall fell on 14 July 2021 as can be seen in Figure 6. Therefore, we will analyse the maximum daily precipitation accumulation in April to September (Apr-Sep; RX1day [mm/day]) for the Ahr and Erft region. For the Belgian Meuse catchment the precipitation leading to the extreme impact accumulated over a longer time frame leading to the analysis of the maximum two-day precipitation accumulation in Apr-Sep (RX2day [mm/day]). Please note that RX2day values are also expressed in [mm/day] which means the accumulation has been averaged over the two days. Multiplication of RX2day with two gives the total amount of rain that fell within 48 hours. For the Pooling Region, we are analysing RX1day as well as RX2day (both for Apr-Sep).
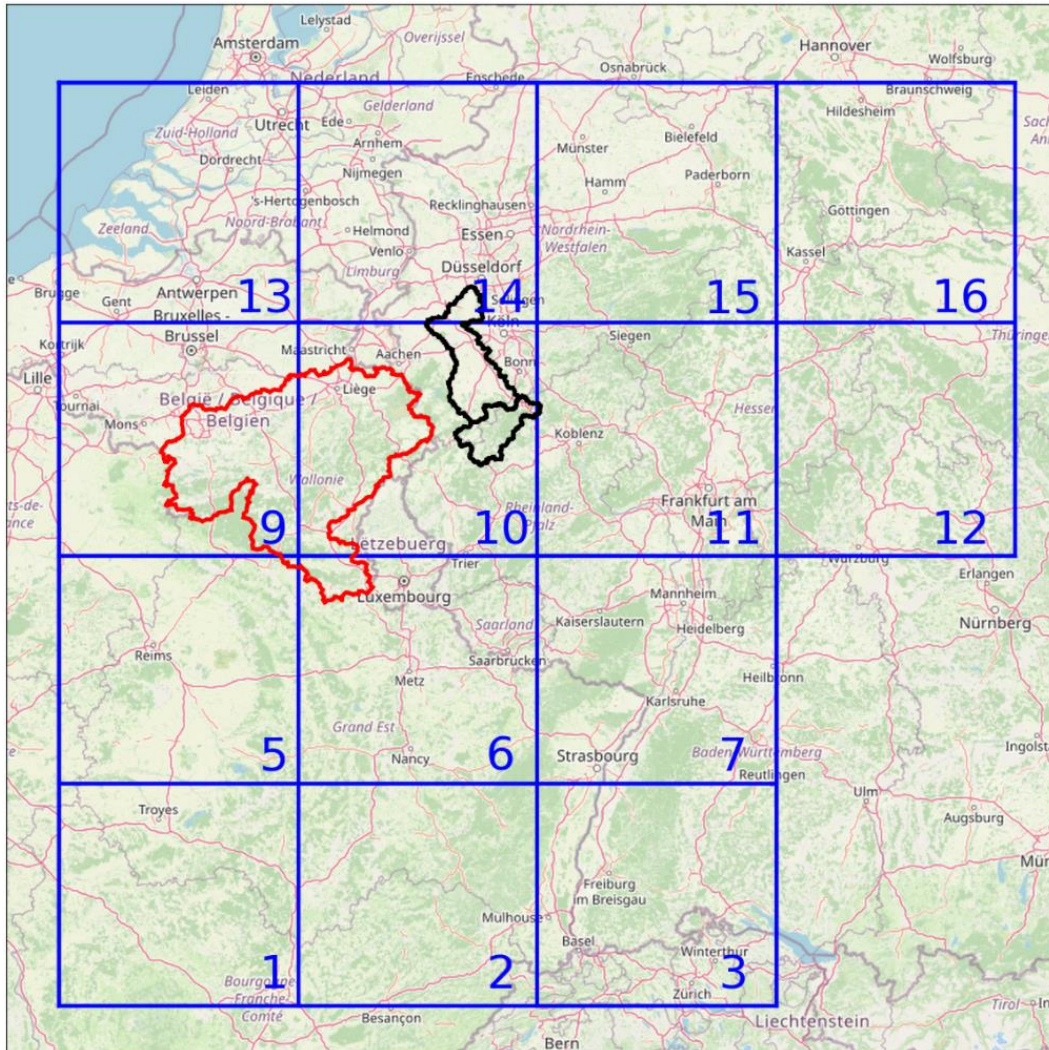
Figure 5: Regions analysed within this study. Area of the Meuse catchment is shown in red, the combined Ahr and Erft catchment shown in black and the tiles/regions used within the pooling approach are shown in blue.

Copyright of underlying map: © OpenStreetMap-Mitwirkende.

The events analysed here are small-scale extremes, and therefore challenging to attribute using climate models with coarse model resolution. Thus, this study does not directly use any Global Climate Model (GCM) simulations and furthermore disregards Regional Climate Models (RCMs) that have a horizontal resolution coarser than 12.5 km, which results in a much smaller set of simulations than is typically used within World Weather Attribution analyses of an event. As a result, we use RCM simulations that have a resolution equal to or finer than 12.5 km, including simulations from EURO-CORDEX which downscale a variety of GCMs. Furthermore some convection-permitting model (CPM) simulations which are not typically used within attribution studies, but can represent small-scale extreme precipitation events more vividly, are included into this study. However, all of these CPM models provide simulations from just one ensemble member and for a fairly limited amount of years (up to 15 decades of data). Probabilistic event attribution is based on solid statistics of extreme values. The limited availability of data for the reasonably small-scale event analysed here makes this attribution

challenging and requires the use of new datasets. In order to broaden the attribution question for such types of events which may occur elsewhere in Western/Central Europe, and to increase statistical significance of trends, the pooled regions approach considers regions of the same order or slightly larger than the areas most-strongly affected by the July 2021 event (~130 km, see Figure 6). The underlying attribution question for the pooling approach is that of the influence of climate change on probability and intensity of similar extreme precipitation events that could occur anywhere in an area from north of the Alps to the Netherlands regardless of the exact location. Time series for each of the 14 tiles are pooled together in the analysis. However, we estimated that, due to spatial correlation, the number of degrees of freedom of the ensemble is not 14 times that of a single tile, but rather 3-4 times only. The pooling approach was also used for extreme precipitation in the Cévennes mountains (Vautard et al., 2015; Zeder and Fischer 2020), albeit using a rain gauge station pooling. By contrast, the spatial-pooling approach is applied here to area-averaged rainfall data for 14 different rectangular tiles, situated between north of the Alps and the Netherlands (see Fig. 5).
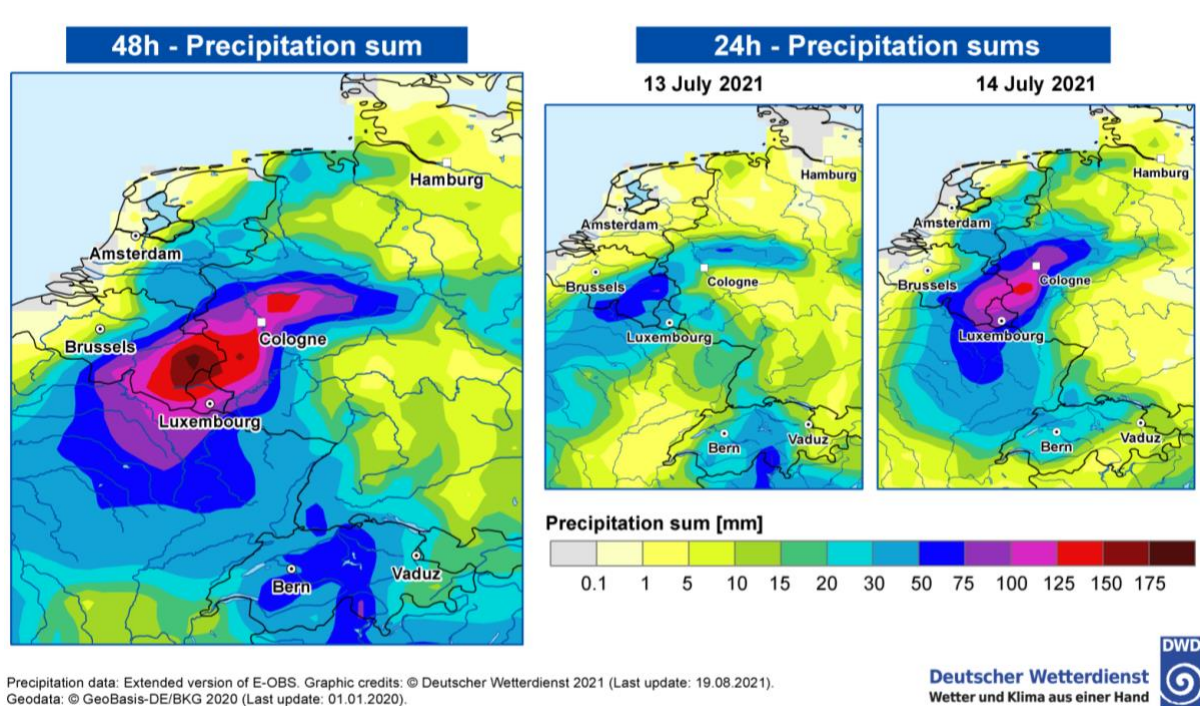
Figure 6: Accumulated precipitation over two days (48h hour accumulation 13 July 00:00 UTC - 15 July 2021, 00:00 UTC) and accumulated over 24 hours for each of the individual days of the extreme precipitation event. The figure is based on an E-OBS dataset extended by numerous stations. For details please refer to Section 2.1.

Independent of the region we focus on the rainfall extremes that occur during the northern hemisphere **summer half-year (April to September)** as the characteristics of extreme precipitation events, as well as the preconditions, such as antecedent precipitation sums and the water holding capacity of the ground, differ between the seasons.

2 Data and methods

2.1 Observational data

2.1.1 E-OBS

E-OBS (version 23.1e), is a 0.25° × 0.25° gridded temperature and precipitation dataset covering Europe, formed from the interpolation of station-derived meteorological observations (Cornes et al., 2018). E-OBS v23.1e was used to produce the climatology and the trend analyses, including the estimates of the return periods. This dataset is used for the model validation for the pooled regions (see Section 4). An enhanced, non-public E-OBS dataset that includes more observational data in the most recent years (mostly additional data starting in 2004 or 2008), and additional data from regional and federal authorities was produced specifically for the analysis of the heavy precipitation discussed here. This enhanced dataset is used to produce maps of the event, however, as it is less homogeneous in time than E-OBS v23.1e, it is less suitable for the trend analyses and estimation of the return periods.

2.1.2 REGNIE

For the Ahr and Erft catchment the REGNIE[6] dataset of DWD is used. REGNIE (Regionalised Precipitation Heights) is a daily gridded precipitation dataset with a resolution of 1 km^2 for Germany derived from station data. It is publicly available for the period since 1st January 1931.

2.1.3 Belgian gridded dataset

For the Belgian Meuse catchment, the observations are interpolated on a grid of 5 km x 5 km. The data used are collected from different observation networks: the Royal Meteorological Institute of Belgium (RMI) climatological raingauge network, the network of Service Publique de Wallonie - Mobilité et Infrastructures (SPW-MI) in Wallonia, and the network of Hydrologisch Informatie Centrum (HIC) of Waterbouwkundig Laboratorium in Flanders. The data were quality controlled by the RMI before interpolation on the grid. The interpolation has been done using a weight as the inverse of the distance to the stations. Time series of 24 stations over Belgium have also been incorporated into the non-public E-OBS dataset.

2.1.4 GISTEMP

As a measure of anthropogenic climate change we use the (4-year low-pass filtered) global mean surface temperature (GMST), where GMST is taken from the National Aeronautics and Space Administration (NASA) Goddard Institute for Space Science (GISS) surface temperature analysis (GISTEMP, Hansen et al., 2010 and Lenssen et al. 2019).

---

[6] Deutscher Wetterdienst, Climate Data Center: REGNIE data set description:
https://opendata.dwd.de/climate_environment/CDC/grids_germany/daily/regnie/DESCRIPTION_gridsgermany_daily_regnie_en.pdf

2.2 Model and experiment descriptions

2.2.1 Regional climate models

2.2.1.1 RACMO

The RACMO regional climate model ensemble was developed at KNMI by downscaling 16 initial-condition realizations of the EC-Earth2.3 coupled climate model in the CMIP5 RCP8.5 scenario (Lenderink et al., 2014). The RACMO model (van Meijgaard et al. 2012) uses a 0.11° (12.5 km) resolution and output includes daily precipitation. RACMO simulations are available for the 1950-2100 period.

2.2.1.2 EURO-CORDEX

A few years ago, the EURO-CORDEX Group defined a framework for the preparation of regional climate projections (Giorgi et al., 2009; Jacob et al., 2014; Jacob et al., 2020). Following this framework, a large number of research institutions and weather services have carried out climate projection runs in various projects. Many simulations were in particular carried out thanks to the PRINCIPLES C3S project, resulting in a set of 75 combinations of 12 RCMs downscaling nine GCMs for the historical period and the RCP8.5 scenario [1951/1971 to 2100] (see Vautard et al. (2021) and Coppola et al. (2021) which describe and assesses the ensemble even though it's size has increased since these publications). However, a subset of these model simulations were first validated based on a comparison of the historical simulation with recent-year observations. For details on the validation see Bayerisches Landesamt für Umwelt (2020), Zier Ch. et al. (2021). Following the conclusions of this evaluation, we removed all simulations downscaling the CanESM and the HadGEM2-ES GCMs. Simulations using the REMO RCM model were also removed. Each simulation was bias corrected using the Cumulative Distribution Function transform method as described in Bartok et al. (2019).

2.2.2 Convection permitting models (CPMs)

The study uses climate simulations from five CPMs: the UK Met Office Unified model (UM), COSMO-CLM, WRF, ALARO-0 and HCLIM38-AROME (HCLIM38). In the following, we will briefly introduce the model simulations and provide information about the driving model scenarios.

The UM simulations are European-wide 2.2km experiments (EUR2.2) from the Met Office Hadley Centre (MOHC). The EUR2.2 runs are designed to be comparable, with 1536x1536 grid points, and span most of Western and Central Europe (~3800x3500km). EUR2.2 integrations are available for a historical period (1998-2008) and a future scenario (10yrs, ~2100 under the RCP 8.5) both based on a HadGEM3 model run.

The HCLIM38 simulations were carried out by the nonhydrostatic model HCLIM38-AROME (Belusic et al. 2020) at 2.5km horizontal resolution on a domain ranging from the UK to Poland and Mid-Italy to Southern Scandinavia. The HCLIM38 simulations consist of three GCM-forced runs (historic 1996-2005, RCP 8.5 2041-2050 and 2090-2099, forced using EC-Earth). HCLIM38 is run in a double-nested way, with RACMO RCM in between the host model and the CPM.

The WRF-ME-3km simulation are from a one-way double-nested WRF v3.6.1 simulation, consisting of a 12.2km EURO-CORDEX domain (EUR-11) and a 3.1km mid-European domain centered over Germany (ME-3km) with 480x456 grid points. The model results used here are from a downscaling of the CMIP5 Earth System Model of the Max-Planck-Institute (MPI-ESM-LR r1i1p1) GCM for three time slices of 12 years each, the historical period (1994-2005), and RCP4.5 projections (2039-2050, 2089-2100). Details of the model configuration, an evaluation of (extreme) precipitation w.r.t. to in-situ observations (using an ERA-Interim driven evaluation run), and a study on future changes of Clausius-Clapeyron scaling are given in Knist et al., 2020.

The ALARO-0 climate projections cover the continuous periods 1950-2100 at 4-km for a wide region centered over Belgium (Termonia et al, 2018) and has undergone thorough validation (Van de Vyver et al., 2021) and investigation (Helsen et al., 2020) with respect to extreme rainfall. The runs were performed in a double (one-way) nesting setup where the Belgian domain was nested in an ALARO-0 run over the EURO-CORDEX domain, which was driven by either CNRM-CM5 (historical, RCP 2.6, RCP 4.5, RCP 8.5). In this attribution study we use RCP 4.5 and RCP 8.5 simulations. The model domain covers the Ahr/Erft region, the Meuse region as well as 7 of the 14 tiles (i.e. 4,5,7,8,10,11,12 of the regions shown in Figure 5).

Several time slice experiments of the COSMO-CLM (https://www.clm-community.eu; Rockel et al., 2008) at convection permitting scales have been analyzed within this study, all using the RCP8.5 emission scenario for the future. At the Karlsruhe Institute of technology (KIT) three simulations at 2.8km horizontal resolution have been conducted, driven by the global earth system models EC-EARTH, HadGEM2, and MPI-ESM-LR respectively (EC-EARTH-KIT, HadGEM2-KIT, MPI-ESM-KIT); the model domain covered the Ahr/Erft region, as well as 7 of the 14 tiles (i.e. 2,3,6,7,10,11,12 of the regions shown in Figure 5). At DWD a simulation at 3km horizontal resolution driven by MIROC-MIROC5 was conducted (DWD-CCLM5-MIROC5) within the first phase of the project „Expertennetzwerk (Network of Experts)" (2016-2019), funded by the German Ministry of Transport and Digital Infrastructure (BMVI); here both small regions and all 14 tiles were covered by the model domain.

As a measure of anthropogenic climate change in the models we use the (4-year low-pass filtered) GMST if we only have one realization of the GMST from the driving GCM model at hand, and an ensemble-mean GMST if several ensemble members are available.

2.3 Statistical methods

A full description of the statistical methods used for this event attribution is given in Philip et al. (2020) and van Oldenborgh et al. (2021). Here we give a summary.

As discussed in the introduction we analyse the Apr-Sep maxima of 1-day and 2-day averaged precipitation (RX1day or RX2day) averaged over the regions defined above. The same analysis is applied and the same metric used for both gridded observational data and climate model output. We follow the steps outlined in the WWA protocol for event attribution (Philip et al. 2020). The analysis steps include: (i) trend calculation from observations; (ii) model validation; (iii) multi-model attribution; and (iv) synthesis of the attribution statement.

For the event under investigation we calculate the return periods, probability ratio (PR) and change in intensity as a function of GMST. The two climate conditions we compared are defined as the current

2021 climate `and a GMST value representative of the climate of preindustrial level, −1.2 ºC relative to 2021 (1850−1900, based on the Global Warming Index https://www.globalwarmingindex.org).` Later we refer to this reference as the past-to-present. To statistically model the selected event, we use a GEV distribution that scales exponentially with GMST, as inspired by the Clausius-Clapeyron relation (See equation 2 in Philip et al., 2020), with location parameter μ and scale parameter σ varying such that their ratio is constant, and a constant shape parameter ξ. These assumptions might be less robust here than in analyses of large-scale precipitation events and they are also less robust when combining annual maxima and much more extreme events. Next, results from observations and from the models are synthesized into a consistent attribution statement. In the validation and trend analysis of model simulations, we use all available model data up to 2030 to study changes between the past and the current climate to increase the availability of data points. Based on the model simulations we additionally analyse the intensity change and PR between a future climate at +2°C above the preindustrial reference, which is equivalent to +0.8°C above the current climate of 2021. Later we refer to this reference as the present-to-future. For this analysis we use all available model data up to the end of the model runs. The decisions on the years included in the analyses deviate somewhat from the standard procedure and are a compromise between the standard procedure, in which we use data up to the present GMST for the past-to-present analysis, and having sufficient data for a good fit. Confidence intervals for the individual model or observation datasets express the statistical-model uncertainty, obtained using a non-parametric bootstrap procedure.

# 3 Observational analysis: return time and trend

3.1 Ahr and Erft catchments

The analysis of the REGNIE dataset for the Ahr and Erft catchment indicates a RX1day precipitation value of 93 mm/day for the 2021 event, see Figure 7. Note, this value is a spatial average over the analysed region. The best estimate of the return period of this event is so large, i.e. in the order of 1 in 15000 yr - much larger than the length of the time series - that we cannot give a precise value, see Figure 8.

Note that the GEV fit to quantify the return period does not include the event itself as the area was chosen as having an extreme event and the extreme value occurring in this year is therefore drawn from a much larger distribution than the historical time series. Whilst we use the best estimate of the return period in the other event definitions, here we opt for the most conservative approach to use the lower return period estimate of 700 years for the model analysis. With this conservative choice, it is possible to analyse observational and model data for the Ahr/Erft region based on a return period that avoids extrapolation too far into the tail of the distribution, which would make results much less reliable and interpretable. From the observational data we can neither prove there is a trend nor prove the absence of a trend as the climate noise is too large, i.e. the fit indicates a change in intensity with a large confidence interval (CI) around zero (95% CI -20% to 29%), and the uncertainty in the probability ratio permits such a large range of values that providing a best estimate is no longer meaningful. The absence of a significant trend at the scale of a small catchment is consistent with theoretical expectations (Li et al. 2020; Aalbers et al. 2018, Fischer et al. 2014) given the very large internal variability and the small spatial scale of the relevant events, which may mask or amplify local trends and prevents robust conclusions about the existence of local trends in this type of precipitation events. At global scale for

most larger subcontinental regions with sufficient observations, an observed increase in heavy precipitation is well established in the literature, including medium confidence in an increase in a larger region including West-Central Europe (IPCC 2021, Chapter 11; Seneviratne et al, in press).
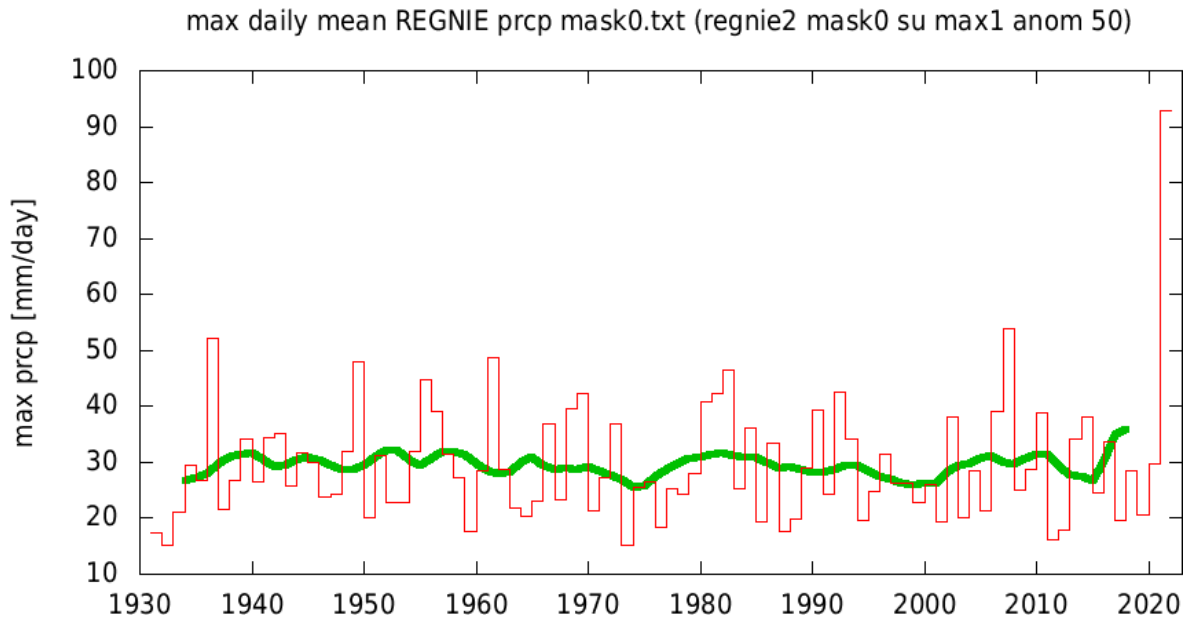
Figure 7: Apr-Sep block maximum of the daily accumulated precipitation (RX1day) of the Ahr/Erft basin-averaged rainfall (red line) and a 10-yr running mean (green line) obtained with the REGNIE dataset. (Data source: Deutscher Wetterdienst, Climate Data Center: https://opendata.dwd.de/climate_environment/CDC/grids_germany/daily/regnie)
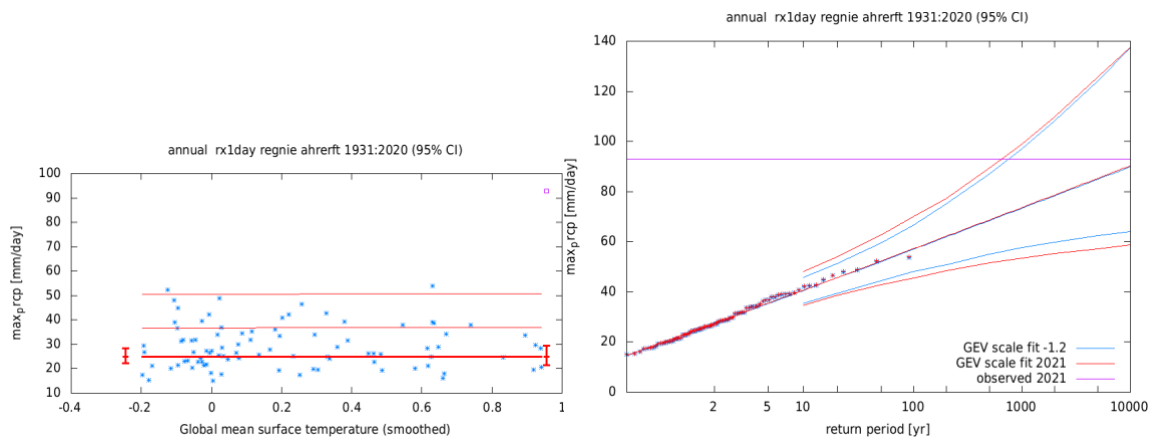

Figure 8: GEV fit with constant dispersion parameters, and location parameter scaling proportional to GMST of the index series for the Ahr/Erft region (based on REGNIE data). Left: the observed RX1day as a function of the smoothed GMST. The thick red line denotes the location parameter, the thin red lines the 6 and 40-yr return times. The July 2021 observation is highlighted with the magenta box. Right: Return time plots for the climate of 2021 (red) and a climate with GMST 1.2 °C cooler (blue). The past observations are shown twice: once scaled up to the current climate and once shifted down to the 1.2 °C cooler climate of the late nineteenth century. The magenta line shows the magnitude of the 2021 event analysed here. No information from 2021 is included to obtain the fit.

## 3.2 Belgian part of Meuse catchment upstream of Eijsden

Over the eastern Belgian part of the Meuse catchment, precipitation accumulation locally reached values up to more than 270 mm/3-day.

The analysis of the two-day precipitation spatially-averaged over this part of the Meuse catchment using the Belgian gridded dataset indicates a value for RX2day of 53 mm/day for 2021 (see Figure 9) with a corresponding return period of about 1000 years (95% CI 200 to 1.2E+05 years, see Figure 10). Similarly to the observational data analysis for the Ahr/Erft region, it is not possible to base a confident statement about the existence or lack of a trend in RX2day for this region on the available observational data, as natural variability is too high compared to the signal on this small scale (see discussion within Section 3.1). Thus, the fit does not indicate a significant change visible over natural variability, with a probability ratio of 0.90 (95% CI 0.17 to 6.27) and a change in intensity of -1.6% (95% CI -20% to 29%). As for the Ahr/Erft catchment the GEV fit does not include the event itself as the area was chosen as having an extreme event. The conclusions from this analysis of the Belgian gridded dataset fully agree with a similar analysis using the enhanced E-OBS data including additional observations as described in Section 2.
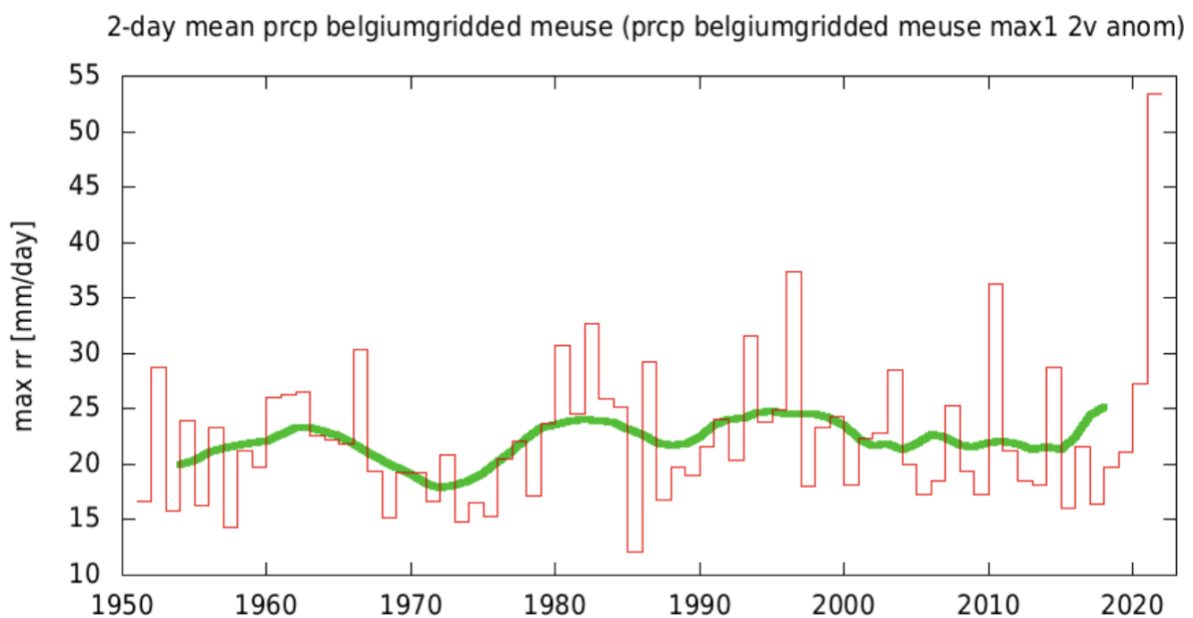
Figure 9: As Fig. 7 but for the gridded Belgian RX2day (2-day average) dataset.
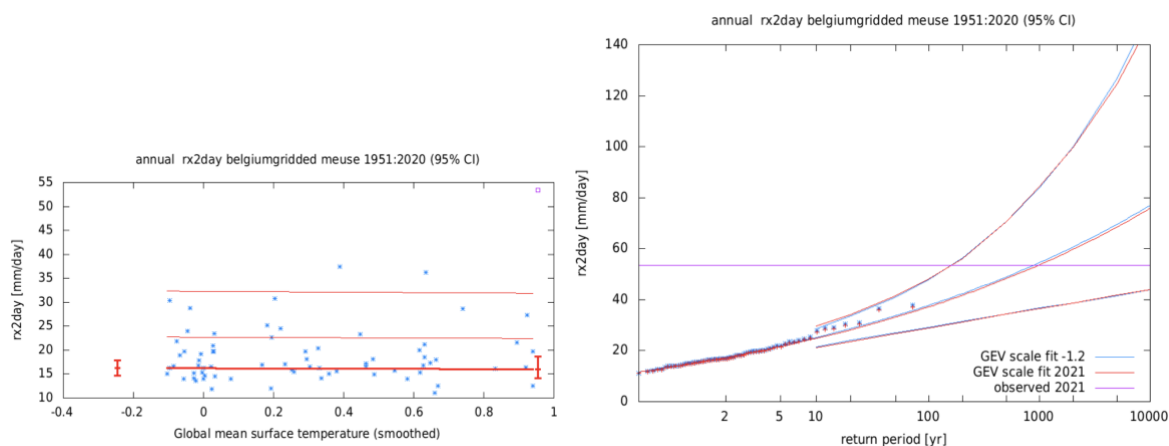
**Figure 10:** As Fig. 8 but for the gridded Belgian RX2day dataset.

3.3 Pooling Region

The individual tiles in the Pooling Region are treated similarly to how several members of an ensemble can be treated when analysing model simulations. The observational analysis indicates a value for RX1day of 64 mm/day for the tile that observed the maximum precipitation within the summer months of 2021 to date (see Figure 11). Fitting of a GEV distribution to the one year block maxima indicates that the tail of the fit behaves differently from the rest (figure not shown here). Therefore, and as we have sufficient data due to the pooling approach, we opt to analyse the extreme values using a block size of 5 years[7] instead of one year that was selected for the analysis of the Ahr/Erft region and for Belgian Meuse catchment. That means we select and study the most extreme value within each tile for every 5-year block. This choice is a compromise between looking further into the tail (larger blocks) and retaining enough data points for a good fit (smaller blocks and therefore more data). The event year was included in the fit, as we do not select the tiles based on the event, rather span a much wider region. Figure 12 shows the GEV fit to the extreme values based on 5-year block maxima. The return period of this event is about 400 years (95% CI 170 to 2500 years).

A return period of 400 years means that you would expect one event per tile per 400 years. That means we would have more than one such event per 400 years in the larger European region (Pool). The fit indicates that there is a significant change in the RX1day index, with a probability ratio of 7.7 (95% CI 2.0 to 52) and a change in intensity of 22% (95% CI 6.7 to 34%). Using other block lengths for the block maxima does not affect the results much.

A similar analysis for RX2day (See bottom rows of Figure 11 and 12), with a value of 45 mm/day, shows similar behavior. Using the 5-year block maxima for the pooled time series indicates a return period of 300 years (95% CI 130 to 1200 years). Again, there is a significant trend towards heavier precipitation, with a probability ratio of 5.9 (95% CI 1.6 to 12) and a change in intensity of 24% (95% CI 7.7 to 30%).

---

[7] 5-year block means here that only the highest value from a 5-year block is used.
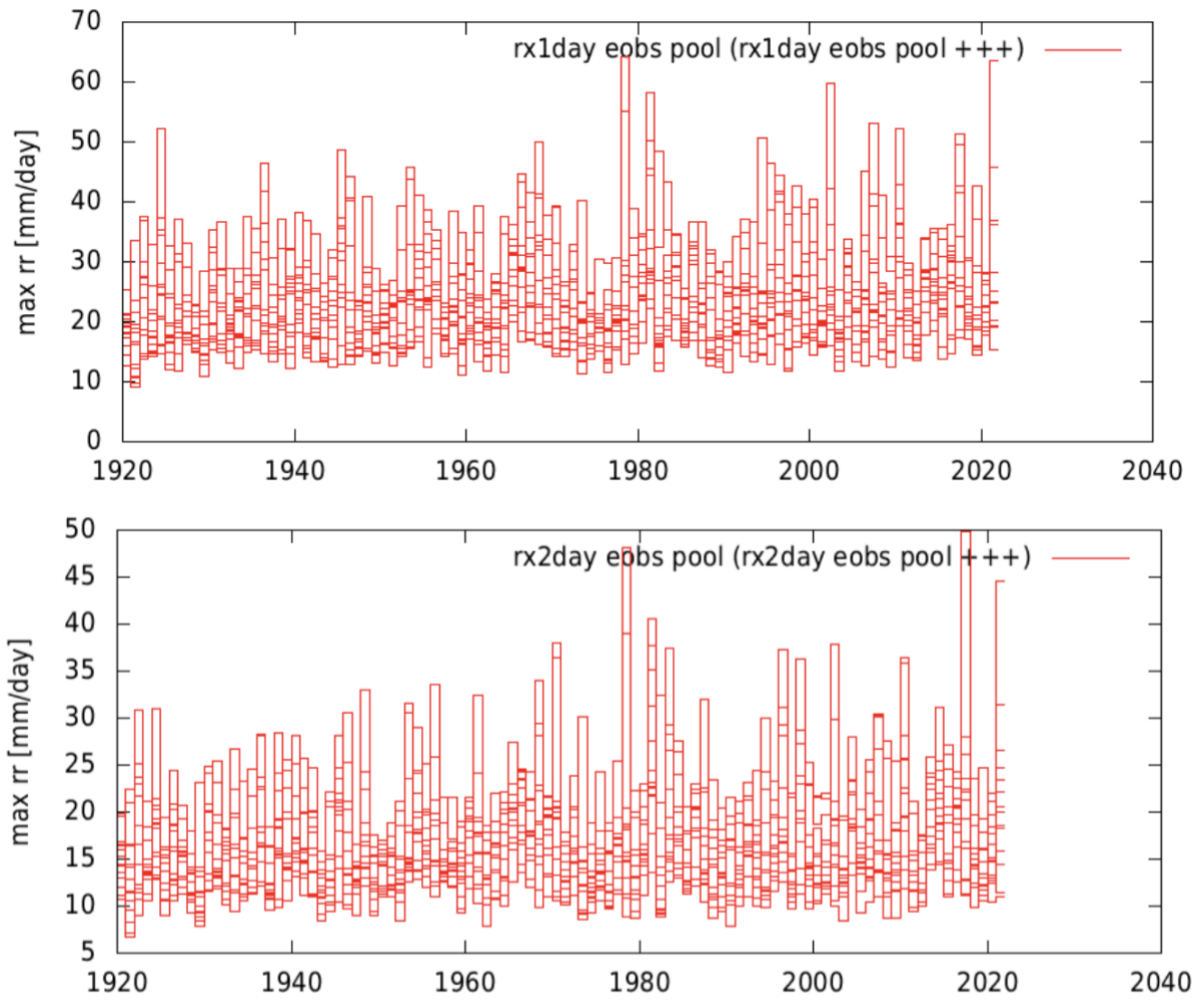
Figure 11: Apr-Sep maximum of the E-OBS RX1day (top) and RX2day (bottom) pooled time series showing 1-year block maxima for all 14 boxes. Source: E-OBS.
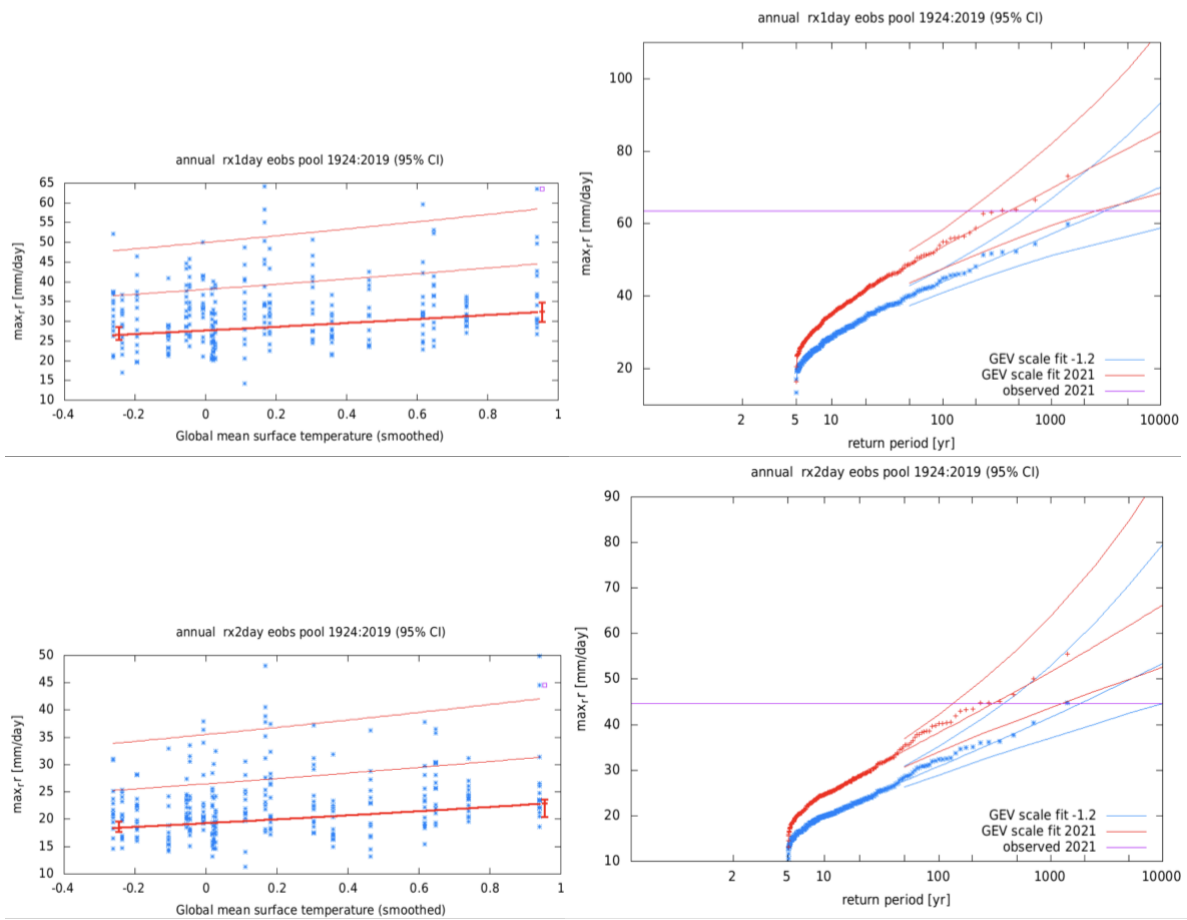
Figure 12: Top: As Fig. 8 but for the pooled E-OBS RX1day dataset with 5-year blocks. Bottom, same but for RX2day. Source: E-OBS.

4 Model evaluation

In this section we show the result of the model evaluation which is performed per region. The tables show the model evaluation results. Any noteworthy detail or decision related to the evaluation are incorporated in a 'comments' column.

The labels for the seasonal cycle are obtained by comparing the timing of the peaks in the seasonal cycle of the daily time series. A similar check on whether the model spatial pattern resembles the observed one has only been done if the spatial pattern was readily available (where this was not possible as part of this rapid study we mark this with a "-" in the respective column). Several of the convection permitting models (HCLIM38, UKMO-CPM2p2, WRF-EUR-11-EURO-CORDEX, WRF-ME-3km) had only ~10 years of historical data available for the historical climate period (here defined as pre-2030), which is insufficient to reliably calculate confidence intervals for the statistical fit parameters. For these models, all data, including the future period, is used for evaluation and to specify the event magnitude from the chosen return period. These models are marked with a star (*) in the evaluation tables here and in the tables showing the results in Section 5. Only results for the present-to-future are calculated for these events. For DWD-CCLM5-MIROC5 only results for the future have been used because results for the past were likely based on a too short time series to achieve reliable results for past changes.

Table 3: Evaluation of the model simulations for the Ahr and Erft.

Model (ensemble members) / Observations	Seasonal cycle	Spatial pattern	Dispersion	Shape parameter	Conclusion
REGNIE, 1931-			0.277 (0.234 ... 0.311)	0.0050 (-0.14 ... 0.13)	
ALARO-0 RCP4.5 (1)	good	-	0.306 (0.247 ... 0.350)	0.12 (-0.074 ... 0.25)	good
ALARO-0 RCP8.5 (1)	good, mean and 97.5 percentile follow same pattern as observed	-	0.303 (0.241 ... 0.346)	0.080 (-0.18 ... 0.21)	good
DWD-CCLM5-MIROC5 (1)	good	-	0.343 (0.245 ... 0.419)	0.12 (-0.086 ... 0.27)	reasonable, high dispersion
EC-EARTH-KIT (1)	reasonable	-	0.282 (0.212 ... 0.342)	0.24 (-0.032 ... 0.40)	reasonable, seasonal cycle and high shape parameter
eurocordex (54)	good	good	0.297 (0.288 ... 0.302)	0.033 (0.012 ... 0.057)	good
HadGEM2-KIT (1)	bad	-	0.271 (0.206 ... 0.316)	0.11 (-0.15 ... 0.25)	bad, seasonal cycle
HCLIM38* (1)	good	-	0.240 (0.167 ... 0.279)	0.027 (-0.24 ... 0.25)	good, future only
MPI-ESM-KIT (1)	reasonable	-	0.228 (0.171 ... 0.282)	0.22 (-0.022 ... 0.38)	reasonable, seasonal cycle and low dispersion
racmo (16)	good	good	0.311 (0.300 ... 0.323)	0.12 (0.078 ... 0.15)	good
UKMO-CPM2p2* (1)	reasonable	-	0.241 (0.106 ... 0.320)	0.13 (-0.12 ... 0.39)	reasonable, high shape, future only
WRF-EUR-11-EURO-CORDEX* (1)	reasonable	-	0.326 (0.239 ... 0.388)	0.086 (-0.073 ... 0.25)	reasonable, seasonal cycle, future only

Model (ensemble members)/ Observations	Seasonal cycle	Spatial pattern			Conclusion
WRF-ME-3km* (1)	good	-	0.331 (0.250 ... 0.395)	0.17 (-0.094 ... 0.34)	reasonable, high dispersion and shape, future only

Table 4: Evaluation of the model simulations for the Belgian Meuse catchment upstream of Eijsden.

Model (ensemble members)/ Observations	Seasonal cycle	Spatial pattern	Dispersion	Shape parameter	Conclusion
BE gridded			0.211 (0.164 ... 0.247)	0.13 (0.0 ... 0.27)	
ALARO-0 RCP4.5 (1)	good	-	0.214 (0.0770 ... 0.247)	0.077 (-0.074 ... 0.21)	good
ALARO-0 RCP8.5 (1)	good	-	0.214 (0.173 ... 0.244)	0.072 (-0.074 ... 0.19)	good
DWD-CCLM5-MIROC5 (1)	good	-	0.213 (0.153 ... 0.252)	-0.0060 (-0.21 ... 0.20)	reasonable, low shape
eurocordex (54)	good	good	0.243 (0.236 ... 0.248)	0.054 (0.033 ... 0.078)	good, seasonal cycle & spatial pattern not provided
HCLIM38* (1)	reasonable	-	0.241 (0.132 ... 0.282)	0.0040 (-0.33 ... 0.32)	reasonable, seasonal cycle, future only
racmo (16)	good	good	0.249 (0.238 ... 0.260)	0.095 (0.055 ... 0.14)	reasonable, high dispersion
UKMO-CPM2p2* (1)	reasonable	-	0.268 (0.141 ... 0.331)	0.086 (-0.19 ... 0.35)	reasonable, high dispersion, future only
WRF-EUR-11-EURO-CORDEX* (1)	good	-	0.218 (0.131 ... 0.271)	0.14 (-0.060 ... 0.40)	good
WRF-ME-3km* (1)	good	-	0.232 (0.151 ... 0.283)	0.093 (-0.20 ... 0.33)	good

Table 5: Evaluation of the model simulations for the Pooled Region, RX1day.

Model (ensemble members)/ Observations	Seasonal cycle	Spatial pattern	Dispersion	Shape parameter	Conclusion
E-OBS			0.223 (0.194 ... 0.243)	-0.010 (-0.12 ... 0.11)	
ALARO-0-rcp45 (1)	reasonable	-	0.227 (0.217 ... 243)	0.12 (0.022 ... 0.22)	reasonable, seasonal cycle, high shape
ALARO-0-rcp85 (1)	good	-	0.234 (0.197 ... 0.251)	0.063 (-0.12 ... 0.19)	good
DWD-CCLM5-MIROC5 (1)	reasonable	-	0.223 (0.174 ... 0.253)	0.10 (-0.071 ... 0.21)	reasonable, seasonal cycle
EC-EARTH-KIT (1)	reasonable	-	0.214 (0.166 ... 0.249)	-0.064 (-0.23 ... 0.089)	reasonable, seasonal cycle
eurocordex (54)	good	good	0.205 (0.198 ... 0.212)	0.024 (0.0080 ... 0.046)	good
HadGEM2-KIT (1)	bad		0.206 (0.140 ... 0.236)	0.14 (0.011 ... 0.33)	bad, bad seasonal cycle, high shape
HCLIM38* (1)	reasonable	-	0.249 (0.200 ... 0.279)	0.085 (-0.029 ... 0.24)	reasonable, seasonal cycle, high dispersion, future only
MPI-ESM-KIT (1)	good	-	0.266 (0.200 ... 0.300)	-0.068 (-0.14 ... 0.12)	reasonable, seasonal cycle
racmo (16)	good	good	0.218 (0.209 ... 0.224)	0.030 (0.0060 ... 0.065)	good
UKMO-CPM2p2* (1)	reasonable	-	0.225 (0.162 ... 0.265)	-0.020 (-0.27 ... 0.19)	reasonable, seasonal cycle, future only
WRF-EUR-11-EURO-CORDEX* (1)	good	-	0.216 (0.169 ... 0.241)	0.10 (-0.065 ... 0.26)	good, future only
WRF-ME-3km* (1)	good	-	0.192 (0.151 ... 0.229)	0.15 (-0.075 ... 0.23)	reasonable, dispersion only good if including future in the validation

Table 6: Evaluation of the model simulations for the Pooled Region, RX2day.

Model (ensemble members) / Observations	Seasonal cycle	Spatial pattern	Dispersion	Shape parameter	Conclusion
E-OBS			0.212 (0.191 ... 0.240)	0.042 (-0.028 ... 0.17)	
ALARO-0 RCP4.5 (1)	reasonable	-	0.254 (0.192 ... 0.265)	0.12 (-0.0010 ... 0.26)	reasonable, seasonal cycle, high dispersion
ALARO-0 RCP8.5 (1)	good	-	0.252 (0.192 ... 0.258)	0.066 (-0.033 ... 0.23)	reasonable, high dispersion
DWD-CCLM5-MIROC5 (14)	reasonable	-	0.217 (0.181 ... 0.247)	0.066 (-0.27 ... 0.13)	good
EC-EARTH-KIT (1)	reasonable	-	0.229 (0.185 ... 0.258)	0.033 (-0.14 ... 0.22)	reasonable, seasonal cycle
eurocordex (54)	good	good	0.212 (0.205 ... 0.219)	0.025 (0.0090 ... 0.047)	good
HadGEM2-KIT (1)	bad	-	0.218 (0.161 ... 0.261)	0.085 (-0.044 ... 0.26)	bad, seasonal cycle
HCLIM38* (1)	reasonable	-	0.217 (0.169 ... 0.246)	0.10 (-0.095 ... 0.23)	reasonable, seasonal cycle, future only
MPI-ESM-KIT (1)	good	-	0.265 (0.203 ... 0.293)	-0.076 (-0.17 ... 0.15)	reasonable, high dispersion, low shape
racmo (16)	good	good	0.225 (0.216 ... 0.234)	0.037 (0.0040 ... 0.066)	reasonable, shape too low, just reasonable
UKMO-CPM2p2* (1)	reasonable	-	0.219 (0.155 ... 0.264)	0.12 (-0.12 ... 0.24)	reasonable, seasonal cycle, future only
WRF-EUR-11-EURO-CORDEX* (1)	good	-	0.196 (0.148 ... 0.218)	0.083 (-0.041 ... 0.22)	good, future only
WRF-ME-3km* (1)	good	-	0.211 (0.158 ... 0.243)	0.061 (-0.057 ... 0.22)	good, future only

5 Multi-model attribution

This section shows probability ratios and change in intensity (ΔI) for models and also includes these values calculated from the fits to the observational data.

Table 7: Analysis results for the Ahr/Erft region showing the model RX1day threshold for a 1-in-1000 year event in the current climate, and the probability ratios and intensity changes for the present climate with respect to preindustrial conditions (1850 to 1900, labelled past-to-present) and for the future climate +2 °C GMST with respect to preindustrial (an additional +0.8 °C GMST to current conditions) future climate, labelled present-to-future. The values for future changes are given with respect to the present.

Model (ensemble members)/ Observations	Threshold	Probability ratio PR [-] past-to-present	Change in intensity ΔI [%] past-to-present	Probability ratio PR [-] present-to-future	Change in intensity ΔI [%] present-to-future
REGNIE, 1931-	92.8 mm	1.1 (0.015 ... ∞)	0.40 (-20 ... 29)		
ALARO-0 RCP4.5 (1)	96 mm	1.9 (0.51 ... 5.8e+2)	11 (-11 ... 41)	1.4 (0.99 ... 2.8)	5.1 (-0.18 ... 9.7)
ALARO-0 RCP8.5(1)	92 mm	3.6 (0.64 ... 1.0e+6)	19 (-7.4 ... 53)	1.1 (0.93 ... 1.5)	1.8 (-1.1 ... 5.1)
DWD-CCLM5-MIROC5 (1)	93 mm			1.5 (1.1 ... 3.9)	5.2 (1.0 ... 9.6)
EC-EARTH-KIT (1)	150 mm	1.2 (0.11 ... 6.7)	4.5 (-18 ... 35)	1.1 (0.93 ... 1.3)	1.4 (-1.6 ... 4.6)
eurocordex (54)	73 mm	1.3 (1.0 ... 1.7)	3.3 (0.17 ... 6.2)	1.3 (1.2 ... 1.3)	2.9 (2.4 ... 3.4)
HCLIM38* (1)	61 mm			0.99 (0.079 ... 4.9)	-0.079 (-5.4 ... 5.3)
MPI-ESM-KIT (1)	120 mm	0.61 (0.053 ... 3.2)	-10 (-24 ... 20)	0.95 (0.75 ... 1.3)	-1.0 (-4.6 ... 2.3)
racmo (16)	84 mm	1.5 (1.1 ... 2.0)	6.7 (2.1 ... 12)	1.2 (1.1 ... 1.3)	2.8 (2.0 ... 3.6)
UKMO-CPM2p2* (1)	77 mm			1.0 (0.63 ... 2.9)	0.074 (-5.4 ... 6.7)
WRF-EUR-11-EURO-CORDEX* (1)	98 mm			0.81 (0.23 ... 3.0)	-3.1 (-19 ... 11)
WRF-ME-3km* (1)	120 mm			1.3 (0.30 ... 4.3)	4.6 (-9.5 ... 15)

Table 8: Analysis results for the Belgian Meuse catchment upstream of Eijsden. Same as Table 7 but for Belgian Meuse catchment RX2day data for a 1-in-700 year event.

Model (ensemble members)/ Observations	Threshold	Probability ratio PR [-] past-to-present	Change in intensity ΔI [%] past-to-present	Probability ratio PR [-] present-to-future	Change in intensity ΔI [%] present-to-future
BE gridded	53.4 mm	0.90 (0.17 ... 6.3)	-1.6 (-20 ... 29)		
ALARO-0 RCP4.5 (1)	52 mm	3.4 (0.89 ... 1.2e+6)	16 (-1.7 ... 38)	1.4 (1.0 ... 3.5)	4.2 (0.41 ... 8.2)
ALARO-0 RCP8.5 (1)	50 mm	1.9 (0.45 ... 68)	7.7 (-7.1 ... 27)	1.4 (1.2 ... 2.9)	3.6 (1.5 ... 5.8)
DWD-CCLM5-MIROC5 (1)	47 mm			1.6 (0.95 ... 49)	4.0 (-0.23 ... 8.4)
eurocordex (54)	86 mm	1.0 (0.82 ... 1.2)	0.46 (-2.2 ... 2.2)	1.2 (1.1 ... 1.2)	1.8 (1.4 ... 2.2)
HCLIM38* (1)	37 mm			1.6 (0.80 ... 18)	4.1 (-2.2 ... 8.5)
racmo (16)	49 mm	1.2 (0.92 ... 1.7)	2.7 (-1.2 ... 6.8)	1.1 (1.1 ... 1.2)	1.6 (0.97 ... 2.2)
UKMO-CPM2p2* (1)	52 mm			1.1 (0.54 ... 25)	1.8 (-4.3 ... 9.8)
WRF-EUR-11-EURO-CORDEX* (1)	61 mm			1.4 (0.45 ... 6.5)	5.3 (-7.1 ... 13)
WRF-ME-3km* (1)	58 mm			1.1 (0.49 ... 32)	1.5 (-7.9 ... 14)

Table 9: Results for the Pooled Region RX1day. Same as Table 7 but for the pooled RX1day data for a 1-in-400 year event.

Model (ensemble members) / Observations	Threshold	Probability ratio PR [-] past-to-present	Change in intensity ΔI [%] past-to-present	Probability ratio PR [-] present-to-future	Change in intensity ΔI [%] present-to-future
E-OBS	63.6 mm	7.7 (2.0 ... 52)	22 (6.7 ... 34)		
ALARO-0 RCP4.5 (1)	71 mm	1.4 (0.65 ... 16)	5.1 (-6.4 ... 29)	1.5 (1.2 ... 2.2)	5.7 (2.6 ... 8.5)
ALARO-0 RCP8.5 (1)	72 mm	2.2 (0.63 ... 1.2e+4)	11 (-6.9 ... 33)	1.3 (1.1 ... 1.8)	3.5 (1.9 ... 5.6)
DWD-CCLM5-MIROC5 (1)	77 mm			1.5 (1.3 ... 1.8)	5.9 (3.7 ... 7.7)
EC-EARTH-KIT (1)	65 mm	1.9 (0.077 ... 49)	5.6 (-11 ... 25)	1.0 (0.54 ... 1.3)	0.061 (-2.8 ... 2.1)
eurocordex (54)	56 mm	1.3 (0.87 ... 1.9)	3.0 (-1.6 ... 7.4)	1.3 (1.2 ... 1.3)	3.3 (3.0 ... 3.6)
HCLIM38* (1)	65 mm			1.3 (1.0 ... 2.2)	4.2 (0.55 ... 8.6)
MPI-ESM-KIT (1)	77 mm	0.65 (0.097 ... 10)	-4.3 (-20 ... 27)	1.2 (0.96 ... 1.4)	2.1 (-0.56 ... 4.5)

racmo (16)	57 mm	1.7 (1.2 ... 2.5)	6.8 (2.2 ... 11)	1.3 (1.2 ... 1.4)	3.2 (2.7 ... 3.7)
UKMO-CPM2p2* (1)	61 mm			0.95 (0.60 ... 8.9)	-0.52 (-5.1 ... 5.4)
WRF-EUR-11-EURO-CORDEX* (1)	73 mm			1.2 (0.56 ... 2.5)	2.4 (-6.5 ... 8.6)
WRF-ME-3km* (1)	73 mm			1.2 (0.81 ... 4.3)	2.8 (-2.8 ... 12)

Table 10: Results for the Pooled Region RX2day. Same as Table 7 but for the pooled RX2day data for a 1-in-300 year event.

Model / Observations	Threshold	Probability ratio PR [-] past-to-present	Change in intensity ΔI [%] past-to-present	Probability ratio PR [-] present-to-future	Change in intensity ΔI [%] present-to-future
E-OBS	44.6 mm	5.9 (1.6 ... 13)	24 (7.7 ... 30)		
ALARO-0 RCP4.5 (1)	52 mm	0.84 (0.32 ... 3.6)	-3.1 (-15 … 20)	1.3 (1.1 ... 2.1)	3.7 (1.0 … 8.3)
ALARO-0 RCP8.5 (1)	50 mm	1.1 (0.32 ... 4.5)	0.74 (-16 … 18))	1.2 (1.1 ... 1.6)	3.1 (1.0 … 5.5)
DWD-CCLM5-MIROC5 (1)	54 mm			1.4 (1.2 ... 1.9)	5.4 (3.2 ... 7.2)
EC-EARTH-KIT (1)	49 mm	0.86 (0.099 ... 2.4)	-1.9 (-17 ... 11)	0.98 (0.68 ... 1.2)	-0.24 (-2.8 ... 2.1)
eurocordex (54)	79 mm	1.2 (0.86 ... 1.8)	2.2 (-1.8 ... 7.2)	1.2 (1.2 ... 1.3)	2.8 (2.6 ... 3.3)
HCLIM38 (1)	45 mm			1.1 (0.90 ... 2.0)	1.9 (-1.7 ... 5.1)
MPI-ESM-KIT (1)	51 mm	0.45 (0.093 ... 8.6)	-8.0 (-18 ... 28)	1.1 (0.92 ... 1.3)	1.6 (-1.2 ... 3.8)
racmo (16)	41 mm	1.7 (1.2 ... 2.6)	6.8 (2.0 ... 12)	1.3 (1.2 ... 1.3)	2.9 (2.4 ... 3.5)
UKMO-CPM2p2 (1)	49 mm			0.88 (0.34 ... 1.3)	-2.2 (-6.8 ... 3.1)
WRF-EUR-11-EURO-CORDEX (1)	49 mm			1.0 (0.55 ... 2.0)	0.56 (-7.0 ... 8.2)
WRF-ME-3km (1)	47 mm			1.0 (0.39 ... 2.6)	0.28 (-8.3 ... 10)

6 Hazard synthesis

For each event definition we calculate the change in intensity as well as the probability ratio of the event in the observations and the models. Only those models that passed the evaluation tests are used. It should be noted here that due to the reasonably small scale of the event, a variety of new models which are not typically part of attribution studies were used. The typical evaluations that are part of the WWA attribution protocol were applied, however, these were designed for simulations on larger scales and further evaluation of the simulations would certainly be beneficial. Thus, the results should be understood as indications of the direction of change, rather than absolute values.

Noting this we synthesise results for the models that pass the evaluation with the observations to give an overarching attribution statement. Observations and models are combined into a single result in two ways if they seem to be compatible. First, we do not account for common model uncertainties beyond the model spread that is depicted by the model average, and compute the weighted average of models and observations: this is indicated by the magenta bar. However, due to common model uncertainties, model uncertainty can be larger than the model spread. Therefore, we also show the more conservative

estimate of an unweighted average of observations and models (i.e. we are not considering the number of models compared to the single observation series), indicated by the white box around the magenta bar in the synthesis figures.

The (uncertainty) values we report combine the two methods we use to estimate uncertainty - the weighted and the unweighted synthesis described above, by taking the largest range. We use this conservative, larger range as we expect it to be more appropriate for small-scale events which are typically more challenging for models to capture. Let's explain the choice we made here a bit further. The synthesis method weights the models by the inverse of the uncertainty range, so large ensembles tend to have smaller uncertainty ranges and a much higher weighting. Where all models can be treated equally this makes sense, but in contrast to other WWA studies, two distinct types of models are used here. We have larger ensembles of regional-scale RCMs and individual simulations of fine-scale CPMs, which are expected to simulate events such as the one analysed here more robustly. Using the standard WWA approach to communicating uncertainties would, however, mean that the results from, and uncertainties, of the convection permitting models are barely taken into account with the risk of providing an overconfident estimate based mainly on the regional models. We therefore decided to use the larger uncertainty range presented by the combination of the magenta and white bars - these larger uncertainty bars were originally only designed to be used in cases where the model and observations disagree due to possible common model errors. For the intensity change the range we get by combining the two bars is similar to the spread you would get when taking only the convection permitting models into account (we have not done the same check for the probability ratio). We acknowledge that the treatment of uncertainties as described here is not ideal. Research on how to synthesize uncertainties for unusual situations is still ongoing, and is necessary to account for the situation encountered here, where we use both CPMs and RCMs to analyse convective events with no preferential consideration. In summary, the combination of both uncertainty bars as we use it in this study gives an indication of the uncertainty range that better reflects the expert judgement on confidence we have in the results, than using the smaller, magenta ranges of uncertainty.

The uncertainties for the present-to-future period are not directly comparable with those calculated for the past-to-present because, aside from including additional models, additional model years, and a smaller change in GMST (-1.2 °C for the past and +0.8 °C for the future), they do not contain observational data and therefore cannot include uncertainty relating to the difference between model and observational results. The uncertainty estimates for the present-to-future comparison are consequently much more reduced in general and may be underestimated as they do not include the information of model/observation trend differences.

It should be noted that an attribution analysis for the small Ahr/Erft and Belgian Meuse regions is challenging based on the available data. Ideally, a long time series of model simulations covering the past as well as the present and future would be used, including several ensemble members. The simulations available for this study are, however, very limited in the length of their time series and only provide one ensemble member per model. For this reason, the results, especially for the small regions, have a large range of values and should be taken as an indication of the direction of change. A more exhaustive discussion on the challenges faced in this study can be found in Section 6.4.

6.1 Ahr and Erft

For the Ahr and Erft, it appears that the observations and models are in good agreement for RX1day. However, the individual uncertainty ranges for the observations and models are generally very large. The synthesized intensity change for the past-to-present (white box, see explanation in Section 6) is -9% to 16%, and for the present-to-future the models indicate an (additional) increase of 1.5% to 4%. A weighted synthesis (magenta bar) of models and observations would give a significant positive trend, but this disregards other uncertainties as pointed out in Section 6.

For the probability ratio the synthesized values for the past-to-present span several orders of magnitude prohibiting a robust statement about the change within this small catchment. For the present-to-future, the model synthesis indicates a minor increase in frequency of about 1.2.
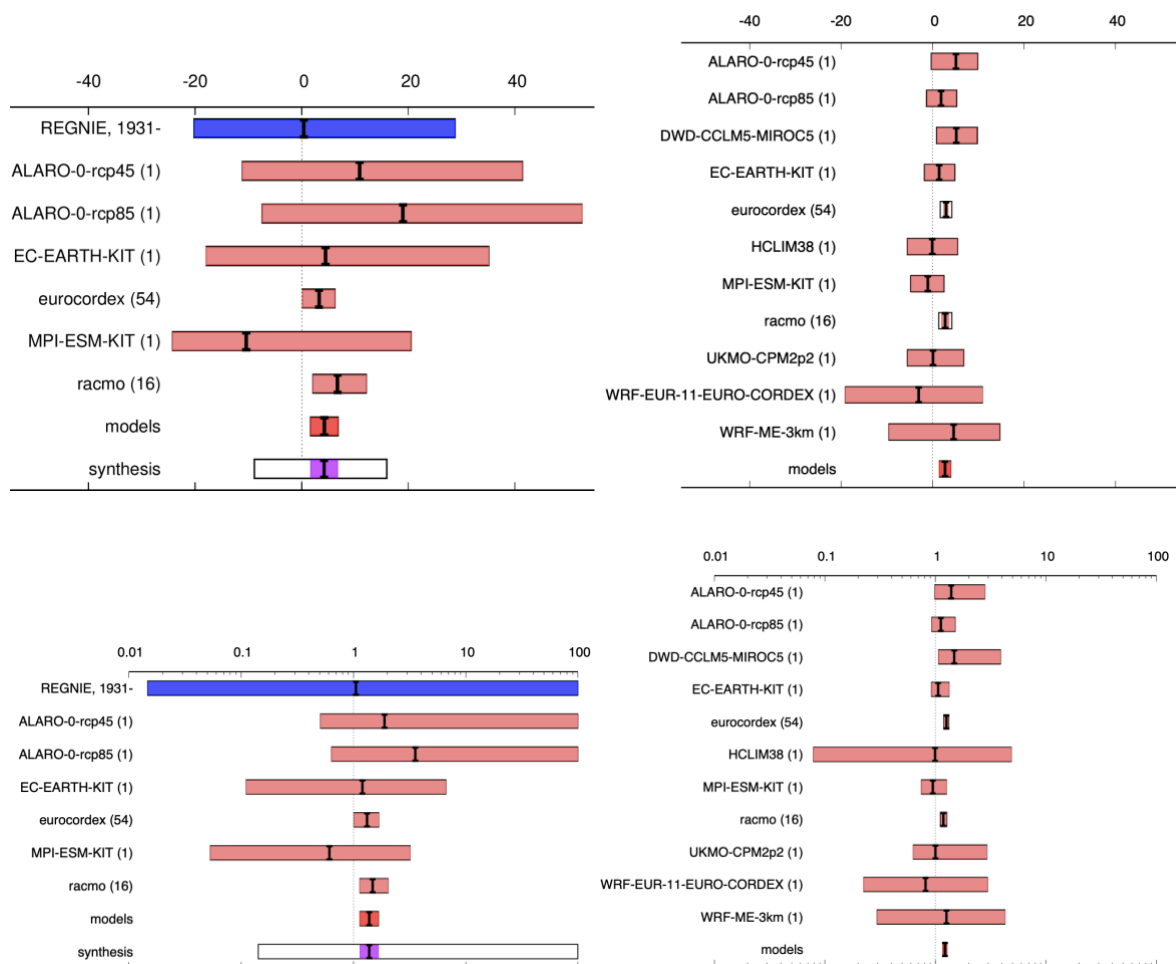
Figure 13: Synthesis of the past-to-present climate (left) and present-to-future climate (right), showing changes in intensity in percent (top) and probability ratios (bottom), for the Ahr/Erft RX1day data. Past-to-present means comparing the 2021 event in the present-day climate with a preindustrial climate (1.2°C cooler than today) and present-to-future means comparing a climate with 2°C of global warming (above preindustrial) with present-day values.

6.2 Belgian Meuse catchment upstream of Eijsden

The synthesized intensity change results for RX2day over the Belgian Meuse catchment are very comparable to those for the Ahr and Erft in their large uncertainty ranges, with a range of -10% to 15% for the past-to-present (white box, see explanation in Section 6), and an increase of 1.5% to 2% for the present-to-future (models only).

The synthesis of the probability ratios indicate a more confined range, compared to the Ahr and Erft, of 0.4 to 3 for the past-to present, but still straddle unity (no change). For present-to-future the models indicate a change of 1.0 to 1.3.
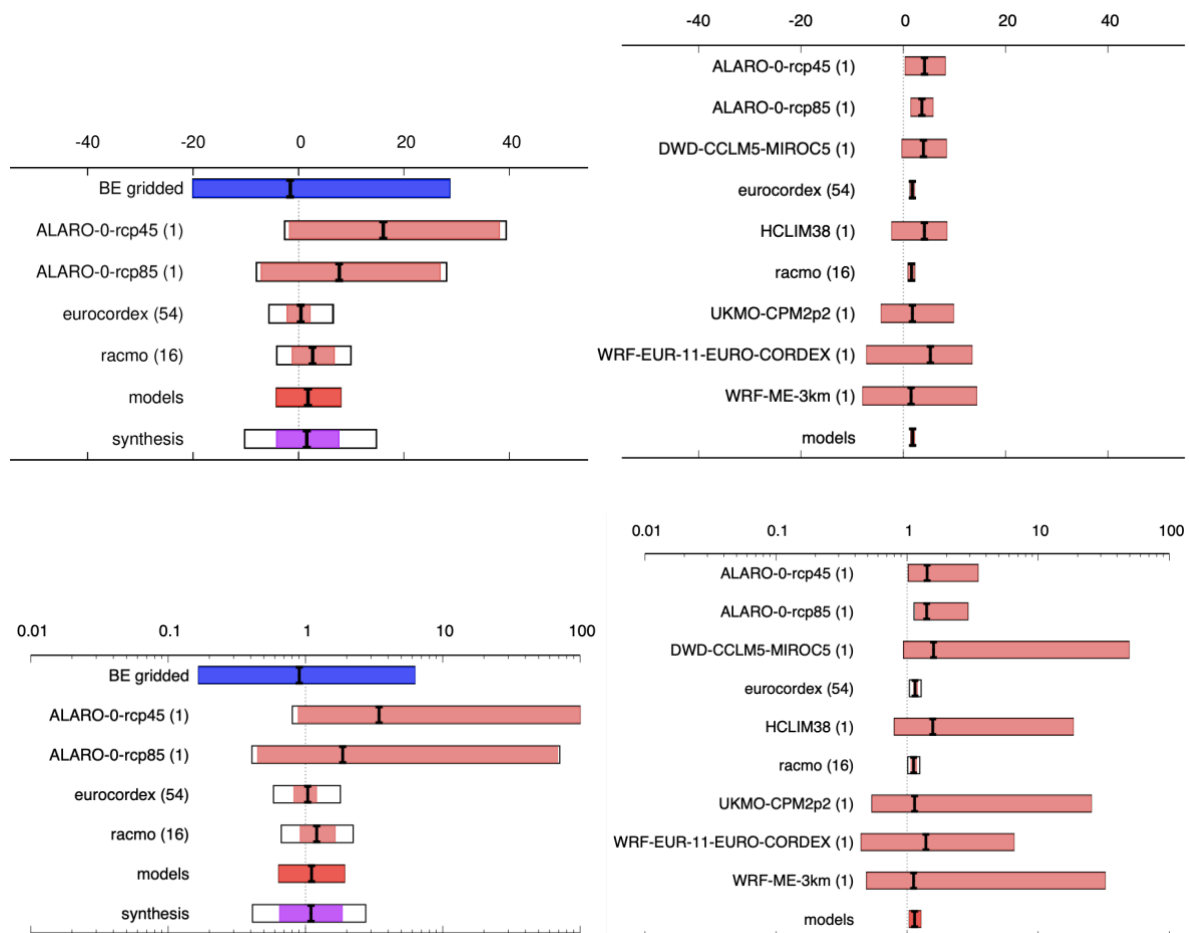
Figure 14: Same as Figure 13 but for RX2day data of the Belgian Meuse catchment upstream of Eijsden. Top: intensity in percent, bottom: probability ratios.

6.3 Pooling Region 1-day precipitation (RX1day)

The synthesized intensity change for RX1day extremes between the past and present occurring in any of the tiles of the pooled region ranges from 3% to 19%, using the larger range of uncertainties, as explained in Section 6, whereas for the present-to-future, the models indicate an intensity change of 0.8% to 6% compared to present. The observational uncertainties are more confined compared to the individual basin results and indicate a significant increase, larger than that from models, but still with some overlap of the uncertainty bounds.

The synthesized probability ratio between past and present lies between 1.2 and 9. For the future compared to present, the models indicate a probability ratio of about 1.3 (range 1.2 to 1.4). Note that we expect the present-to-future uncertainty which comes from model analysis only to be smaller than the past-to-present uncertainty (see text above).
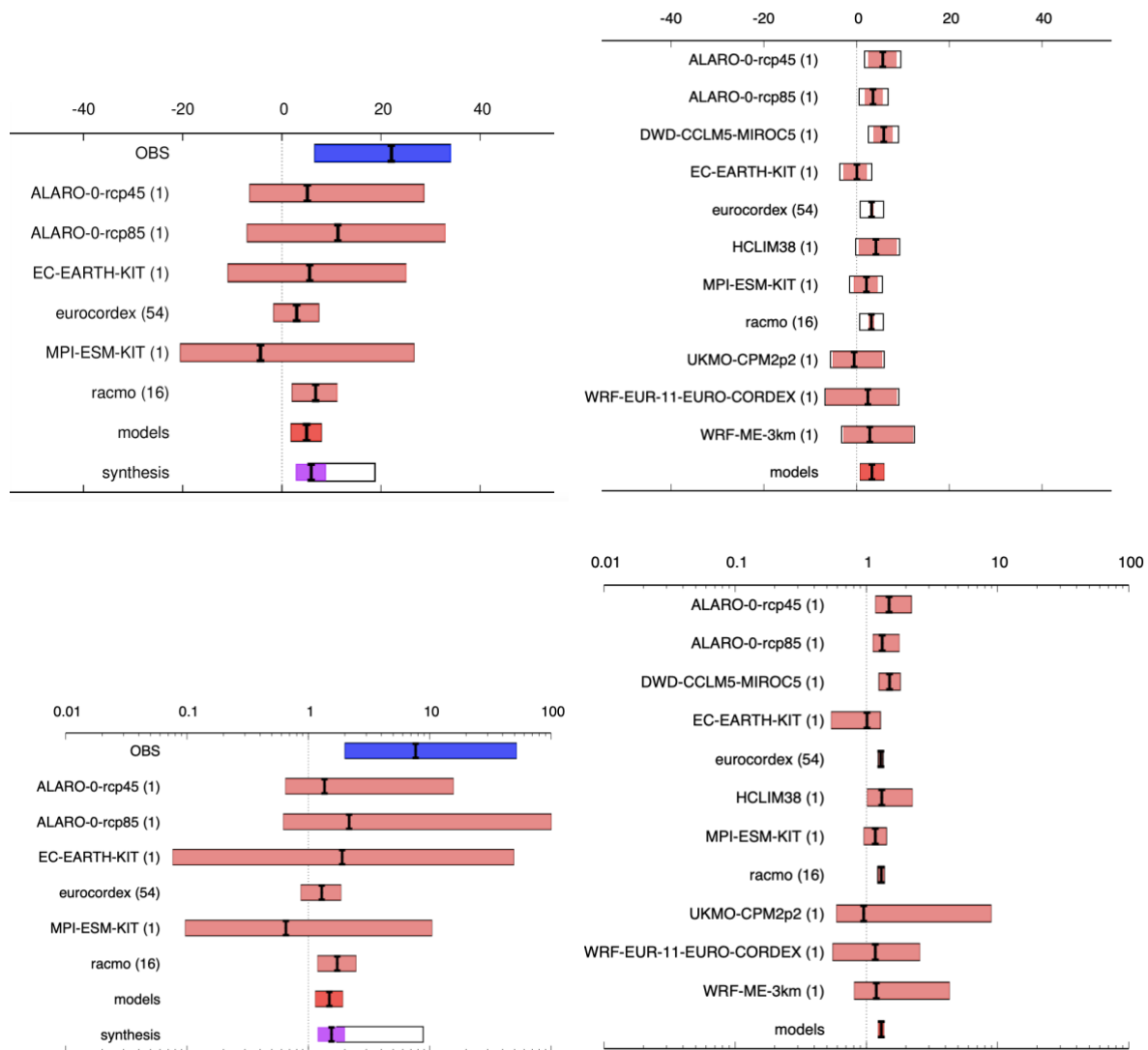
Figure 15: Same as Figure 13 but for RX1day data of the Pooling Region. Top: intensity in percent, bottom: probability ratios.

6.4 Pooling Region 2-day precipitation (RX2day)

The RX2day results are generally very similar to the RX1day results for the pooled region. For RX2day extremes, the intensity change for the past-to-present ranges from 2% to 17%, using the larger range of uncertainties, as explained in Section 6, and for the future the models indicate an increase of 0.2% to 5%.

The synthesized probability ratio between past and present is between 1.5 and 7. For the future models compared to the present, models indicate a probability ratio of 1.1 to 1.4. As for RX1day results, the observations tend to show more significant positive changes than the models and act to extend the upper range of the unweighted synthesis to higher values.
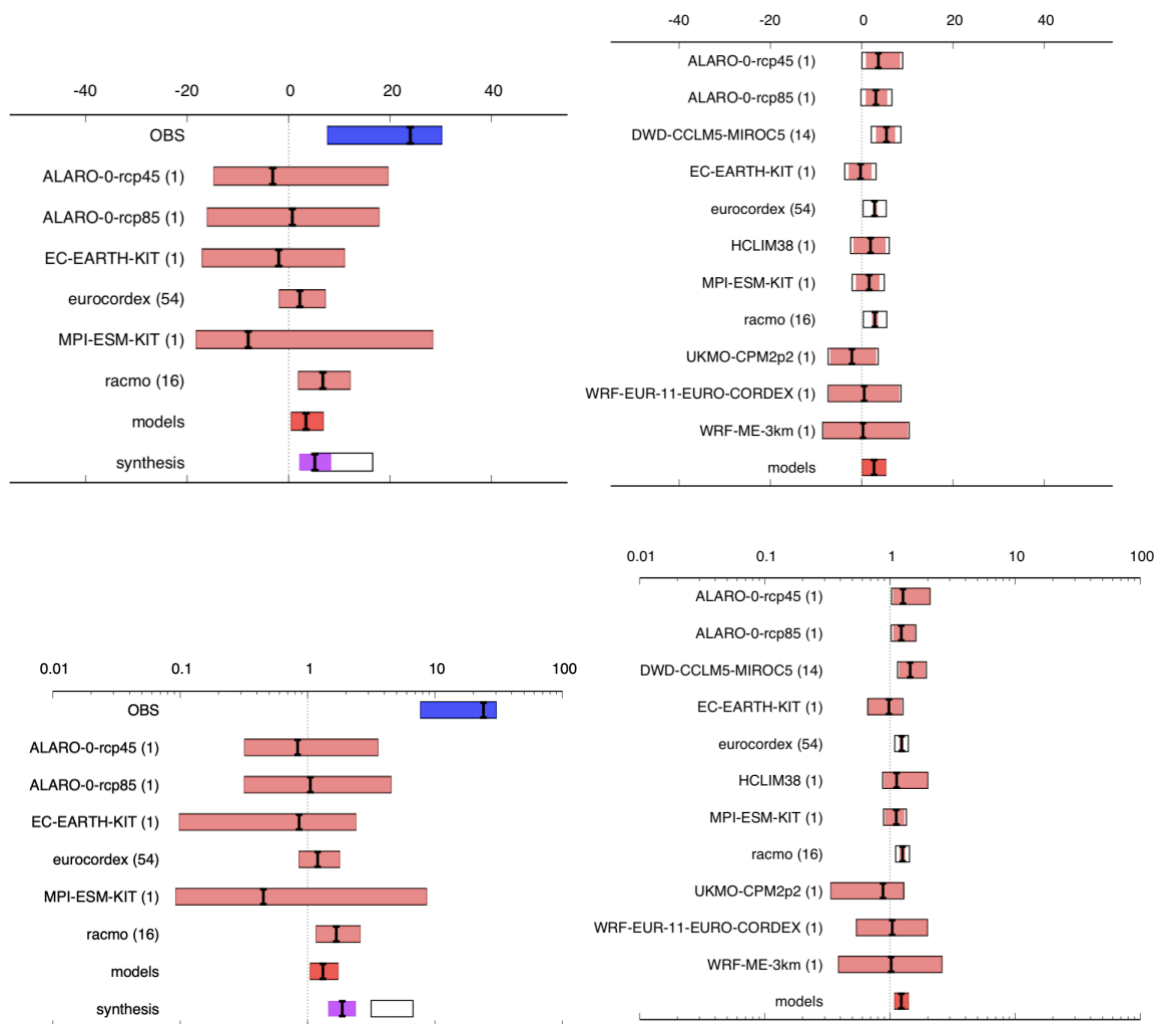
Figure 16: Same as Figure 13 but for RX2day data of the Pooling Region. Top: intensity in percent, bottom: probability ratios.

6.5 Interpretation of results

First of all it should be reiterated that the detection and attribution of trends is challenging for events occuring on such a small scale as the ones which are investigated here. Thus, this study pushes the limits of what current methods of extreme event attribution are designed for.

The floods that struck Germany and Benelux on 14 and 15 July 2021 were caused by persistent convective showers embedded into a larger scale cut-off low pressure system. From a meteorological perspective, this implies a large diversity of scales and processes involved. At the larger scale – 200 km and beyond and the daily time scale – synoptic atmospheric dynamics leading to the low pressure system lingering over Germany set the background atmospheric conditions. Embedded in the frontal system associated with the low pressure system, convective showers strongly affected by atmospheric mesoscale dynamics – at scales typically between 1 and 100 km and time scales ranging from minutes to half a day – cause relatively local and high precipitation rates. Even more so, these time and spatial scales interact (Fowler et al., 2021). Given the high atmospheric humidity at the time of the event – typical values of dew point of 18 degrees and integrated water vapor content of 40-45 kg/m^2 (estimated from ERA5 reanalysis) – this interaction is particularly strong (Lenderink et al., 2017). Thereby convection can also alter the large-scale conditions in a way that promotes further moisture convergence and instability of the atmosphere.

From a flood perspective the importance of the diversity in scales is also apparent. The high discharge of the Meuse relates to the rain accumulations over a large area for approximately two days, yet the more flash flood type event in e.g. Ahr is governed by processes at sub-daily to daily time scales, where rainfall intensities exceed the soil water infiltration speed for rather small catchments. At the same time, pre-conditioned wet soils resulting from the anomalously high accumulated precipitation in the weeks preceding the events likely played a role as well. For this reason, the link between precipitation extremes and extreme discharges is rather complex, and extreme precipitation is often only one factor that may contribute to an extreme flood (Sharma et al., 2018). This is in particular relevant as observational as well as modelling evidence points at altered spatial structures of convective rainfall with warming (Wasko et al., 2015; Lochbihler et al., 2019, 2021), potentially increasing the amount of rainfall at rates beyond the infiltration capacity of the soil and thereby increasing the flood risk more than expected based on accumulation sums only (Sharma et al., 2018).

From a climate modelling perspective, the diversity in time and spatial scales, implies there is no optimal modelling stream to do an attribution analysis. GCMs only capture the large-scale dynamics of this event, while the convective dynamics are strongly simplified and rainfall intensity is spread out over unrealistically large areas due to the lack of sufficient resolution. RCMs – like in the EURO-CORDEX set – have rather realistic large-scale atmospheric dynamics and can be integrated long enough to achieve statistically robust results. Yet, they still suffer from unresolved dynamics related to convective precipitation – they use strongly simplified schemes to represent convective rain called parameterizations which they usually share with the GCMs – which suffer from large biases in convective rain statistics, like the intensity of extremes and the diurnal cycle (Ban et al., 2021). This is in particular worrisome as the latent heat release caused by convection feeds back onto the larger scales (Nie et al., 2018; Lenderink et al., 2017). Finally, CPMs resolve the largest convective dynamics, and have much better statistics of convective rain (Ban et al. 2021; Kendon et al. 2017), but are still relatively unexplored, and runs are typically too short to establish robust statistics and detect climate change signals (unless large areas are pooled together). The fact that the event has both large-scale

features as well as the pronounced small-scale (convective) features, however, makes spatial pooling challenging.

Nevertheless, the change in absolute humidity of the atmosphere is robustly represented in all modelling streams. Although actual increases in humidity do not always follow the local temperature changes using the Clausius-Clapeyron relationship of 6-7 % per degree, observations show (Byrne and O'Gorman, 2018; https://www.metoffice.gov.uk/hadobs/monitoring/humidity.html) and models project robust increases in humidity of the atmosphere. This provides a firm basis of observed and projected increases in precipitation extremes (Fischer et al., 2016). Typically expected changes in near surface humidity are 4-6 % per degree global warming (O'Gorman and Muller, 2010; Lenderink and Attema, 2015; Lenderink et al., 2021), depending on precipitation-soil moisture drying feedback in summer over the continent. Nonetheless, since heavy precipitation events occur during wet conditions, an increase of about 7 % per degree of global warming, consistent with the Clausius-Clapeyron relationship is overall projected on land (IPCC 2021, Chapter 11: Seneviratne et al., in press). This provides a physically-based baseline estimate of changes to precipitation extremes. Most of the presented trends here are consistent with this estimate. Since 1950 observed annual maximum daily precipitation (RX1day) has intensified at a rate remarkably consistent with the Clausius-Clapeyron relationship of ca. 7% per degree warming aggregated across global land regions (Westra et al., 2013; Sun et al., 2021) as well as across all of Europe (Fischer et al., 2016) and central Europe (including Netherlands, Germany, Austria and Switzerland) (Zeder and Fischer, 2020).

Changes in large-scale and small-scale atmospheric dynamical processes, and other physical processes (like extensive soil drying) may cause deviations from this Clausius Clapeyron behavior (directly tied to the humidity increase). At larger scales, latent heat release may amplify moisture convergence through large-scale lifting (Nie et al., 2018), which has shown to affect increases in precipitation extremes across the globe (Pfahl et al., 2017). At local scales mesoscale convective dynamics (only dynamically resolved by the CPMs) can cause dependencies of precipitation extremes that are twice as large as the increase in humidity, and this behavior strongly depends on the changes in atmospheric stability (temperature lapse rate) and large-scale dynamics (Lenderink et al. 2021; Loriaux et al. 2013). Observed trends in hourly extremes in the Netherlands exceed the Clausius-Clapeyron prediction (Lenderink and Attema, 2015) and appear to co-occur with relatively small changes in atmospheric stability and circulation (Lenderink et al., 2019). These high sensitivities might be consistent with the relatively high trend estimate obtained here from the pooled E-OBS data. But, this also appears to conflict with the stronger changes to stability and circulation in future projections (Brogli et al., 2019; Lenderink et al., 2021). A systematic underestimation of the sensitivity of precipitation extremes to global warming in CMIP5 when confronted with observations has also been found (Borodina et al., 2017).

It is inherently difficult to detect potential local trends in very rare and extreme events such as the heavy precipitation events analyzed here. Based on large climate model ensembles it has been demonstrated that trends in heavy precipitation at the scale of grid points and small catchments can strongly differ between realizations of the exact same model but starting from different atmospheric initial conditions (Li et al. 2020; Aalbers et al. 2018). Thus, even 100-yr long trends at the scale of stations or small catchments may be strongly affected by the chaotic nature of internal climate variability and deviate from the forced response, i.e. the signal in the absence of internal variability, which will emerge in the long run. Therefore, trends at the scale of small catchments should be expected to vary between

individual model simulations and observations simply by chance. Likewise, they may not be representative of the exact long-term local changes that determine the change in the statistically expected event probability.

Therefore, spatial pooling is applied here to reduce the role of internal variability and thereby increase the signal-to-noise ratio. Across large spatial scales the sample size of rare events is substantially higher and a climate signal can be more robustly detected even in comparatively short observational records or model simulations. Spatial pooling has been found to yield signals that are substantially more robust across different observational data sets and model simulations but cannot account for potential small-scale differences in the heavy precipitation response to warming as discussed above.

Concluding, large uncertainty still exists due to i) rather poor signal to noise ratios in observed trends given ii) the rareness of the event and the combination of both large-scale and small-scale features, and iii) the lack of appropriate models that both represent convective dynamics as well as cover sufficiently long time spans. Also, this is further complicated by uncertainty in the appropriate rainfall statistics, and how they relate to the observed floods, in particular for the smaller catchments like the Ahr/Erft. Potential changes to the spatial/temporal distribution of rainfall (intensity) could lead to stronger increases in flash flood risk than estimated based on rainfall accumulation only. Yet, robust increases in humidity do provide a first order estimate of the expected rainfall increases, although the magnitude is quite uncertain.

7 Vulnerability and exposure

Risk, as defined by the IPCC, is the interplay between a hazard, exposure and vulnerability to an extreme event (IPCC, 2014). In the disaster literature, disaster risk is defined as the potential loss of life, injury, or destroyed or damaged assets which could occur to a system, society or a community in a specific period of time, determined probabilistically as a function of hazard, exposure, vulnerability and capacity (UNDRR[8]). Recent research suggests expanding risk analyses to account for cascading and compounding impacts on socio-economic outcomes (Raymond et al., 2020, Balch et al., 2020). Therefore, we use this section to explore the interaction of the hazard within the environment it occurred via the lens 1. vulnerable people, 2. flood protection, and 3. early warning, and raise issues for further research. Given this is a recent disaster, after-action reviews are ongoing and thus we cannot draw final conclusions, but rather focus on synthesising relevant factors for the whole region affected.

The July 2021 floods resulted in extreme impacts including over two hundred deaths, damage to homes, businesses, roads, and other critical infrastructure. Water and electricity supply was disrupted and medical care was under strain with many clinics and pharmacies damaged (DRK[9]). For instance, in Belgium, 37,137 households lost access to electricity and reports from 31 communities indicate that 153 houses were destroyed, 3,025 partly destroyed and 195 dangerously damaged or are to be demolished[10]. With precipitation return times varying from 1 in 300 years to 1 in 1000 years, and peak flow return times of 1 in more than 500 years (Ahr), depending on the geographic area and time period

---

[8] https://www.undrr.org/terminology/disaster-risk
[9] https://www.drk.de/hilfe-in-deutschland/flutkatastrophe-drk-hilfseinsatz-in-deutschland/#c68419
[10] Crisiscenter Belgium, 19.08.2021

used, it is clear this is a very extreme event that is reasonably likely to cause negative impacts. However, especially if events like this may occur more frequently in the future, examining the vulnerability and exposure context becomes critical to reducing future impacts.

7.1 Vulnerable people

Differences in vulnerability and exposure can arise from non-climate factors such as multi-dimensional inequalities and result in differential impacts for vulnerable individuals and households (IPCC, 2014). Drivers of social vulnerability to floods have been discussed extensively in academic literature and include demographics, socioeconomic characteristics, health, risk perception, and coping capacity among others (Rufat et al. 2015). The most vulnerable demographics to flood events are generally thought to be children, older people, and persons with disabilities as these groups may be less aware of risk, have more difficulty self-evacuating, require further assistance by emergency response teams, and may be more difficult to reach (Lowe et al. 2013; Rufat et al. 2015). The population of people over 65 years of age is 18.5% and growing in the Wallonia region of Belgium and also increasing in Germany (Eurostat[11], Statistik[12]). However, a full review of the demographics of the flood victims is not yet available at the time of writing and is required to fully understand the differential impacts faced by vulnerable populations.

7.2 Flood protection

Past experience with floods has shaped protection measures in the region. The Flood Protection Act of 2009, implementing the European Community Floods Directive of 2007 on national level, indicates three primary risk levels for land-use planning nationally: floods with high probability, floods with medium probability, defined as a return time of at least 1 in 100 years and low probability floods, with a return time of at least 1 in 200 years. The Flood Protection Act stipulates that flood risk maps must be developed by 2013, updated by 2019 and revised thereafter once every six years. Following this process, it was mandated that flood risk management plans be developed with an objective to reduce the potential impacts for both medium and low probability flood events, where proportionally relevant. This included updated building codes. The Flood Protection Act also prohibits certain actions that can increase vulnerability and exposure to flood events; this includes guidelines on hazardous materials, preventing individual actions that could impede water flow, mandating environmental conservation considerations and ensuring that community efforts do not adversely affect upstream or downstream communities. The fixed cycle to review and update flood maps and associated plans is also key to managing risks associated with a changing climate (e.g. German Water Resources act, chapter 73 §2, no (6)).

In Rhineland-Palatinate and North Rhine-Westphalia, flood risk maps have been developed for most of the rivers including the Ahr and the Erft (Landesamt für Umwelt, Rheinland-Pfalz, 2021; Landesamt für Natur, Umwelt und Verbraucherschutz, Nordrhein-Westfalen). However, even the chosen "extreme" scenario with low probability was overtopped by the current event in some regions. This paper conservatively estimates the peak flow return time of the Ahr flood event at 1 in > 500 years.

---

[11] https://www.statistiekvlaanderen.be/en/population-by-age-and-gender-0
[12] https://www.statistik.rlp.de/no_cache/de/gesellschaft-staat/bevoelkerung-und-gebiet/pressemitteilungen/einzelansicht/news/detail/News/3121/

In Germany, many flood protection measures (e.g. dike relocations, polders) are coordinated in the 'national flood protection programme' (Federal Ministry of the Environment, 2014). In the Netherlands, municipalities created flood buffer zones, lowered floodplains, engaged in channel dredging and widening, and enacted specific zoning laws (Rijkswaterstaat, 2021[13]). In Belgium, the strategies of flood prevention, mitigation and defence (collectively, Water Systems Arrangement) are the purview of the regional governments, while the Flood Preparation and Flood management functions (relating to emergency planning and crisis management, and insurance, respectively) are governed at the federal level (Mees, H. et al. 2016). Implementation of these measures aid in reducing vulnerability and exposure.

7.3 Early Warning

Extreme rainfall resulted in riverine and flash flooding in towns in Germany, Belgium, the Netherlands, and other countries. This is a complex transboundary event, spanning multiple rivers and countries in Western Europe, with different flood forecasting and early warning structures. Early warning systems are a key factor in flood preparedness. A full after-action review of the event and systems in place is required to properly highlight good practices and diagnose potential areas for improvement in the system. In this section we give a factual overview of the existing systems and possible areas for further study at the time of writing.

Flood forecasting and warning structures vary between European countries. Germany, Belgium, and the Netherlands have national and sub-national early warning systems which communicate flood warnings to local authorities, relevant agencies, and the public. For example, in Germany, flood forecasts are issued by the 16 federal states, based on weather forecasts of Deutscher Wetterdienst. Early warning messages are transmitted in several ways to local authorities and people, including warning apps such as NINA (Federal Office for Civil Protection and Disaster Assistance, 2021), "Meine Pegel" (Flood control centers of the Federal States, 2021) or KatWarn (Fraunhofer Institute for Open Communicating Systems, 2021).

The event of July 2021 was generally well captured by the forecasting and warning system. For example, the forecasting system of the State Office for the Environment, Rhineland-Palatinate issued a warning at Jul 14, 15:26 with a water level of 5.19 m for the gauge Altenahr/Ahr, already much higher than the highest water level on record before (3.71 m, in 2016). The highest warning level was transmitted at 17:17 h via the warning apps and other media. Tshe high warning level also continued during an intermediate forecast of a little lower water levels (4.06 at 18:25). At 19:57 a water level of 6.81 m was forecasted which was very close to the real water level of about 7 m that occured in the early morning of Jul 15 and almost doubled the value of 2 June 2016 (Landesamt für Umwelt, Rheinland-Pfalz, 2019).

---

[13] https://www.rijkswaterstaat.nl/water/waterbeheer/bescherming-tegen-het-water/maatregelen-om-overstromingen-te-voorkomen/ruimte-voor-de-rivieren

Across the affected regions there are ongoing after-action reviews to learn from the event with respect to future risk management. Further research is required to determine if and which factors (e.g. coordination, hazard monitoring, communication systems, public awareness) could be improved to reduce impacts in future extreme floods, especially in the face of rising risks.

8 Data availability

Most of the precipitation data analysed here are available via the Climate Explorer, where we have specifically set up a site that provides model and observational data used in this study, see https://climexp.knmi.nl/ardennen_eifel_floods_timeseries.cgi.

- Climate data of Deutscher Wetterdienst (time series from German weather stations, gridded data for Germany, etc.) is available under an open data licence at DWD's open data server: https://opendata.dwd.de/climate_environment/CDC (for a general introduction see: https://opendata.dwd.de/climate_environment/CDC/Readme_intro_CDC_ftp.pdf). Parts of these data are integrated in the Climate Explorer.

- Data from SPW-MI (Service Publique de Wallonie - Mobilité et Infrastructures, Belgium) is taken from:

- http://voies-hydrauliques.wallonie.be/opencms/opencms/fr/hydro/Archive/annuaires/index.html

- ERA5 data can be obtained through the Copernicus Climate Change Service Climate Data

- Store (CDS) from the Copernicus Climate Change Service (C3S).

- Hydrological data, Netherlands: https://waterinfo.rws.nl/

- Hydrological data Walloon region, Belgium: http://voies-hydrauliques.wallonie.be/opencms/opencms/fr/hydro/Actuelle/crue/cruetableau.do?id=38

- Hydrological statistical yearbook, Germany: http://www.dgj.de/

- Hydrological data Rhineland-Palatinate: https://gda-wasser.rlp-umwelt.de/

- Hydrological data North Rhine-Westphalia: https://luadb.lds.nrw.de/LUA/hygon/pegel.php?interaktiv=P

- Hydrological data Germany (major rivers): https://www.pegelonline.wsv.de/ and m1-datenstelle@bafg.de

- Hydrological projections, Germany: https://ws-klimaportal.bafg.de/

9 Acknowledgements

Here we would like to thank people who contributed to this attribution study in the background, without whom this analysis would not have been possible. The order is purely random.

10 References

Aalbers, E. E., Lenderink, G., van Meijgaard, E., and van den Hurk, B. J. J. M.: Local-scale changes in mean and heavy precipitation in Western Europe, climate change or internal variability?, Climate Dynamics, 50, 4745-4766, doi:10.1007/s00382-017-3901-9, 2018.

Ban, N., and Coauthors, 2021: The first multi-model ensemble of regional climate simulations at kilometer-scale resolution, part I: evaluation of precipitation. Clim. Dyn., 57, 275–302, https://doi.org/10.1007/s00382-021-05708-w.

Balch, J. K., Iglesias, V., Braswell, A. E., Rossi, M. W., Joseph, M. B., Mahood, A. L., et al. (2020). Social-environmental extremes: Rethinking extraordinary events as outcomes of interacting biophysical and social systems. Earth's Future, 8, e2019EF001319. https://doi.org/10.1029/2019EF001319

Bartok, B., Tobin, I., Vautard, R., Vrac, M., Jin, X., Levavasseur, G., ... & Saint-Drenan, Y. M. (2019). A climate projection dataset tailored for the European energy sector. Climate services, 16, 100138.

Bayerisches Landesamt für Umwelt (2020): Das Bayerische Klimaprojektionsensemble – Audit und Ensemblebildung. Umwelt Spezial, Augsburg, 2020. (german)

Borodina, A., E. M. Fischer, and R. Knutti (2017), Models are likely to underesti- mate increase in heavy rainfall in the extratropical regions with high rainfall intensity, Geophys. Res. Lett., 44, 7401–7409, doi:10.1002/2017GL074530.

Bretherton, C. S., M. Widmann, V. P. Dymnikov, J. M. Wallace, and I. Bladé, 1999: The effective number of spatial degrees of freedom of a time-varying field. J. Climate, 12, 1990–2009.

Brogli, R., N. Kröner, S. L. Sørland, D. Lüthi, and C. Schär, 2019: The role of hadley circulation and lapse-rate changes for the future European summer climate. J. Clim., 32, 385–404, https://doi.org/10.1175/JCLI-D-18-0431.1.

Byrne, M. P., and P. A. O'Gorman, 2018: Trends in continental temperature and humidity directly linked to ocean warming. Proc. Natl. Acad. Sci. U. S. A., 115, 4863–4868, https://doi.org/10.1073/pnas.1722312115.

Coppola, E., Nogherotto, R., Ciarlo', J. M., Giorgi, F., van Meijgaard, E., Kadygrov, N., ... & Wulfmeyer, V. (2021). Assessment of the European climate projections as simulated by the large EURO-CORDEX regional and global climate model ensemble. Journal of Geophysical Research: Atmospheres, 126(4), e2019JD032356.

Cornes, R., G. van der Schrier, E.J.M. van den Besselaar, and P.D. Jones. (2018). An Ensemble Version of the E-OBS Temperature and Precipitation Datasets, J. Geophys. Res. Atmos., 123. doi:10.1029/2017JD028200.

Duong, D. Q., Hatz, M., Maurer, T. (2021). Ad-hoc Rückrechnung der Hochwasserwelle der Ahr vom 14./15.7.2021 an der Rheinmündung durch Vergleich von Messwerten und Ergebnissen hydrodynamischer Simulation der Wasserstände und Abflüsse an den Rheinpegeln Andernach, Oberwinter und Bonn. BfG-report unpublished, BfG, Koblenz.

Federal Office for Civil Protection and Disaster Assistance (2021): NINA. Notfall-Informations- und Nachrichten-App des Bundes. https://www.bbk.bund.de/DE/Warnung-Vorsorge/Warn-App-NINA/warn-app-nina_node.html

Federal Ministry of the Environment BMU (2014): Nationales Hochwasserschutzprogramm https://www.bmu.de/download/nationales-hochwasserschutzprogramm/

Fischer, E. M., and R. Knutti, 2016: Observed heavy precipitation increase confirms theory and early models. Nat. Clim. Chang. 6, 986–991, https://doi.org/10.1038/nclimate3110.

Flood control centers of the Federal States (2021): Meine Pegel. https://play.google.com/store/apps/details?id=de.hochwasserzentralen.app

Fowler, H. J., and Coauthors, 2021: Anthropogenic intensification of short-duration rainfall extremes. Nat. Rev. Earth Environ., 2, 107–122, https://doi.org/10.1038/s43017-020-00128-6.

Fraunhofer Institute for Open Communicating Systems (2021): Katwarn. https://www.katwarn.de/en/

Giorgi, F., Jones, C., & Asrar, G. R. (2009). Addressing climate information needs at the regional level: the CORDEX framework. *World Meteorological Organization (WMO) Bulletin*, *58*(3), 175.

Hansen, J., Ruedy, R., Sato, M., and Lo, K. (2010). Global surface temperature change. Rev. Geophys., 48, RG4004, doi:10.1029/2010RG000345.

Helsen, S., van Lipzig, N. P., Demuzere, M., Broucke, S. V., Caluwaerts, S., De Cruz, L., De Troch, R., Hamdi, R., Termonia, P., Van Schaeybroeck, B., Wouters, W., 2020. Consistent scale-dependency of future increases in hourly extreme precipitation in two convection-permitting models, Climate Dynamics 54, 1267–1280. doi:10.1007/s00382-019-05056-w

Hersbach, H, Bell, B, Berrisford, P, et al. The ERA5 global reanalysis. Q J R Meteorol Soc. 2020; 146: 1999– 2049. https://doi.org/10.1002/qj.3803

IPCC, 2014: Climate Change 2014: Synthesis Report. Contribution of Working Groups I, II and III to the Fifth Assessment Report of the Intergovernmental Panel on Climate Change [Core Writing Team, R.K. Pachauri and L.A. Meyer (eds.)]. IPCC, Geneva, Switzerland.

IPCC, 2021: Climate Change 2021: The Physical Science Basis. Contribution of Working Group I to the Sixth Assessment Report of the Intergovernmental Panel on Climate Change [Masson-Delmotte, V., P. Zhai, A. Pirani, S. L. Connors, C. Péan, S. Berger, N. Caud, Y. Chen, L. Goldfarb, M. I. Gomis, M. Huang, K. Leitzell, E. Lonnoy, J.B.R. Matthews, T. K. Maycock, T. Waterfield, O. Yelekçi, R. Yu and B. Zhou (eds.)]. Cambridge University Press. In Press

Jacob, D., J. Petersen, B. Eggert, A. Alias, O. B. Christensen, L. M. Bouwer, A. Braun, A. Colette, M. Déqué, G. Georgievski, E. Georgopoulou, A. Gobiet, L. Menut, G. Nikulin, A. Haensler, N. Hempelmann, C. Jones, K. Keuler, S. Kovats, N. Kröner, S. Kotlarski, A. Kriegsmann, E. Martin, E. van Meijgaard, C. Moseley, S. Pfeifer, S. Preuschmann, K. Radtke, D. Rechid, M. Rounsevell, P. Samuelsson, S. Somot, J.-F. Soussana, C. Teichmann, R. Valentini, R. Vautard, B. Weber, and P. Yiou, 2014, EURO-CORDEX: New high-resolution climate change projections for European impact research, Regional Environmental change, 14, 563-578.

Jacob, D., C. Teichmann, S. Sobolowski, E. Katragkou, I. Anders, M. Belda, R. Benestad, F. Boberg, E. Buonomo, R. M. Cardoso, A. Casanueva, O. B. Christensen, J. H. Christensen, E. Coppola, L. De Cruz, E. L. Davin, A. Dobler, M. Domínguez, R. Fealy, J. Fernandez, M. Á. Gaertner, M. García-Díez, F. Giorgi, A. Gobiet, K. Goergen, J. J. Gómez-Navarro, C. Gutiérrez, J. M. Gutiérrez, I. Güttler, A. Haensler, T. Halenka, S. Jerez, P. Jiménez-Guerrero, R. G. Jones, K. Keuler, E. Kjellström, S. Knist, S. Kotlarski, D. Maraun, E. van Meijgaard, P. Mercogliano, J. P. Montávez, A. Navarra, G. Nikulin, N. de Noblet-Ducoudré, H.-J. Panitz, M. Piazza, E. Pichelli, J.-P. Pietikäinen, A. F. Prein, D. Rechid, B. Rockel, R. Romera, E. Sánchez, K. Sieck, P. M.M. Soares, S. Somot, L. Srnec, S. L. Sørland, P. Termonia, H. Truhetz, R. Vautard, K. Warrach-Sagi, V. Wulfmeyer, Regional climate downscaling over Europe: perspectives from the EURO-CORDEX community, Regional Environmental Change (2020), (20)2.

Junghänel, T., P. Bissolli, J. Daßler, R. Fleckenstein, F. Imbery, W. Janssen, F. Kaspar, K. Lengfeld, T. Leppelt, M. Rauthe, A. Rauthe-Schöch, M. Rocek, E. Walawender, E. Weigl (2021): Hydro-klimatologische Einordnung der Stark- und Dauerniederschläge in Teilen Deutschlands im Zusammenhang mit dem Tiefdruckgebiet „Bernd" vom 12. bis 19. Juli 2021. Deutscher Wetterdienst, Offenbach am Main. https://www.dwd.de/DE/leistungen/besondereereignisse/niederschlag/20210721_bericht_star kniederschlaege_tief_bernd.html

Kendon, E. J., and Coauthors, 2017: Do Convection-Permitting Regional Climate Models Improve Projections of Future Precipitation Change? Bull. Am. Meteorol. Soc., 98, 79–93, https://doi.org/10.1175/BAMS-D-15-0004.1.

Knist, S., Goergen, K. & Simmer, C. Evaluation and projected changes of precipitation statistics in convection-permitting WRF climate simulations over Central Europe. Clim Dyn 55, 325–341 (2020). https://doi.org/10.1007/s00382-018-4147-x

Kollet, S.J. and Maxwell, R.M. (2006). Integrated surface-groundwater flow modeling: a free-surface overland flow boundary condition in a parallel groundwater flow model. Advances in Water Resources, 29(7), 945-958,

Kollet, S.J. and Maxwell, R.M. (2008). Capturing the influence of groundwater dynamics on land surface processes using an integrated, distributed watershed model.Water Resources Research, 44(2), W02402, doi:10.1029/2007WR006004

Kuffour, B. N. O., Engdahl, N. B., Woodward, C. S., Condon, L. E., Kollet, S., & Maxwell, R. M. (2020). Simulating coupled surface–subsurface flows with ParFlow v3.5.0: capabilities, applications, and ongoing development of an open-source, massively parallel, integrated hydrologic model. Geosci. Model Dev., 13(3), 1373-1397. https://gmd.copernicus.org/articles/13/1373/2020/

Landesamt für Natur, Umwelt und Verbraucherschutz, Nordrhein-Westfalen (2021): Hochwassergefahrenkarten und Hochwasserrisikokarten. https://www.flussgebiete.nrw.de/hochwassergefahrenkarten-und-hochwasserrisikokarten-8406

Landesamt für Umwelt, Rheinland-Pfalz (2019): Deutsches Gewässerkundliches Jahrbuch, Pegel Altenahr. https://fachdaten-wasser.rlp-umwelt.de/mdat_wasser/pegel/dgj/2718040300.pdf?v1

Landesamt für Umwelt, Rheinland-Pfalz (2021): Hochwassergefahren- und Hochwasserrisikokarten. https://hochwassermanagement.rlp-umwelt.de/servlet/is/8662/

Lenderink, G., and J. Attema, 2015: A simple scaling approach to produce climate scenarios of local precipitation extremes for the Netherlands. Environ. Res. Lett., 10, 085001, https://doi.org/10.1088/1748-9326/10/8/085001.

Lenderink, G., van den Hurk, B. J. J. M., Tank, A. M. G. K., van Oldenborgh, G. J., van Meijgaard, E., de Vries, H., and Beersma, J. J.: Preparing local climate change scenarios for the Netherlands using resampling of climate model output, Environmental Research Letters, 9, 115 008, doi:10.1088/1748-9326/9/11/115008, 2014.

Lenderink, G., R. Barbero, J. M. Loriaux, and H. J. Fowler, 2017: Super-Clausius–Clapeyron Scaling of Extreme Hourly Convective Precipitation and Its Relation to Large-Scale Atmospheric Conditions. J. Clim., 30, 6037–6052, https://doi.org/10.1175/JCLI-D-16-0808.1.

Lenderink, G., H. de Vries, H. J. Fowler, R. Barbero, B. van Ulft, and E. van Meijgaard, 2021: Scaling and responses of extreme hourly precipitation in three climate experiments with a convection-permitting model. Philos. Trans. R. Soc. A. Math. Phys. Eng. Sci., 379, 20190544, https://doi.org/10.1098/rsta.2019.0544.

Lenderink, G., D. Belušić, H. J. Fowler, E. Kjellström, P. Lind, E. van Meijgaard, B. van Ulft, and H. de Vries, 2019: Systematic increases in the thermodynamic response of hourly precipitation extremes in an idealized warming experiment with a convection-permitting climate model. Environ. Res. Lett., 14, 074012, https://doi.org/10.1088/1748-9326/ab214a.

Lenssen, N., Schmidt, G., Hansen, J., Menne, M., Persin, A., Ruedy, R., and Zyss, D. (2019). Improvements in the GISTEMP uncertainty model. J. Geophys. Res. Atmos., 124(12), 6307-6326, doi:10.1029/2018JD029522.

Li C, Sun Y, Zwiers F, Wang D, Zhang X, Chen G, Wu H (2020) Rapid warming in summer wet bulb globe temperature in China with human-induced climate change. J Climate 33(13):5697–5711. https://doi.org/10.1175/JCLI-D-19-0492.1

Lochbihler, K., G. Lenderink, and A. P. Siebesma, 2019: Response of Extreme Precipitating Cell Structures to Atmospheric Warming. J. Geophys. Res. Atmos., 2018JD029954, https://doi.org/10.1029/2018JD029954.

Lochbihler, K., G. Lenderink, and A. P. Siebesma, 2021: Cold Pool Dynamics Shape the Response of Extreme Rainfall Events to Climate Change. J. Adv. Model. Earth Syst., 13, 1–16, https://doi.org/10.1029/2020MS002306.

Loriaux, J. M., G. Lenderink, S. R. De Roode, and a. P. Siebesma, 2013: Understanding Convective Extreme Precipitation Scaling Using Observations and an Entraining Plume Model. J. Atmos. Sci., 70, 3641–3655, https://doi.org/10.1175/JAS-D-12-0317.1.

Lowe, D.; Ebi, K.L.; Forsberg, B. Factors Increasing Vulnerability to Health Effects before, during and after Floods. Int. J. Environ. Res. Public Health 2013, 10, 7015-7067. https://doi.org/10.3390/ijerph10127015

Mees, H, Suykens, C, Beyers, J.C, Crabbé, A, Delvaux, B, Deketelaere, K, 2016, Analysing and evaluating flood risk governance in Belgium. Dealing with flood risks in an urbanised and institutionally complex country, STAR-FLOOD Consortium, University Antwerp, KU Leuven, Belgium. ISBN: 978-94-91933-06-6

Nie, J., A. H. Sobel, D. A. Shaevitz, and S. Wang, 2018: Dynamic amplification of extreme precipitation sensitivity. Proc. Natl. Acad. Sci., 115, 9467–9472, https://doi.org/10.1073/pnas.1800357115.

Nilson, E. and Iber, C. (2020): Hochwasser und Klimawandel: Sind wir sicher? Gemeinde und Stadt 11/2020. 325-328 (german)

O'Gorman, P. A., and C. J. Muller, 2010: How closely do changes in surface and column water vapor follow Clausius–Clapeyron scaling in climate change simulations? Environ. Res. Lett., 5, 025207, https://doi.org/10.1088/1748-9326/5/2/025207.

Pfahl, S., P. A. O'Gorman, and E. M. Fischer, Understanding extreme precipitation. Nat. Clim. Chang.,.2017

Philip, S., Kew, S., van Oldenborgh, G. J., Otto, F., Vautard, R., van der Wiel, K., King, A., Lott, F., Arrighi, J., Singh, R., and van Aalst, M. (2020). A protocol for probabilistic extreme event attribution analyses, Adv. Stat. Clim. Meteorol. Oceanogr., 6, 177–203, https://doi.org/10.5194/ascmo-6-177-2020.

Raymond, C., Horton, R.M., Zscheischler, J. et al. Understanding and managing connected extreme events. Nat. Clim. Chang. 10, 611–621 (2020). https://doi.org/10.1038/s41558-020-0790-4

Rockel, B., A. Will, A. Hense, 2008: The regional climate model COSMO-CLM (CCLM). Meteorol. Z. 17, 347–348, doi:10.1127/0941-2948/2008/0309.

Roggenkamp T. & J. Herget (2014): Reconstructing peak discharges of historic floods of the River Ahr, Germany. Erdkunde Vol. 68 · No. 1. 49-59.

Roggenkamp T. & J. Herget (2015): Historische Hochwasser der Ahr. Die Rekonstruktion von Scheitelabflüssen ausgewählter Ahr-Hochwasser. Heimatjahrbuch Kreis Ahrweiler 2015. 150 - 154

Rufat S., Tate E., Burton Ch. B., Maroof A. S. (2015):Social vulnerability to floods: Review of case studies and implications for measurement, International Journal of Disaster Risk Reduction, Volume 14, Part 4, doi.org/10.1016/j.ijdrr.2015.09.013

Seneviratne, S.I., X. Zhang, M. Adnan, W. Badi, C. Dereczynski, A. Di Luca, S. Ghosh, I. Iskandar, J. Kossin, S. Lewis, F. Otto, I. Pinto, M. Satoh, S.M. Vicente-Serrano, M. Wehner, and B. Zhou, in press: Chapter 11: Weather and Climate Extreme Events in a Changing Climate. In: IPCC, 2021: *Climate Change 2021: The Physical Science Basis. Contribution of Working Group I to the Sixth Assessment Report of the Intergovernmental Panel on Climate Change* [Masson-Delmotte, V., P. Zhai, A. Pirani, S. L. Connors, C. Péan, S. Berger, N. Caud, Y. Chen, L. Goldfarb, M. I. Gomis, M. Huang, K. Leitzell, E. Lonnoy, J.B.R. Matthews, T. K. Maycock, T. Waterfield, O. Yelekçi, R. Yu and B. Zhou (eds.)]. Cambridge University Press. In Press

Sharma, A., C. Wasko, and D. P. Lettenmaier, 2018: If Precipitation Extremes Are Increasing, Why Aren't Floods? Water Resour. Res. 54, 8545–8551, https://doi.org/10.1029/2018WR023749.

Sun, Qiaohong, Xuebin Zhang, Francis Zwiers, Seth Westra, and Lisa V. Alexander. "A global, continental, and regional analysis of changes in extreme precipitation." Journal of Climate 34, no. 1 (2021): 243-258.

Tafel, M, Szolnoki, G. Estimating the economic impact of tourism in German wine regions. Int J Tourism Res. 2020; 22: 788– 799. https://doi.org/10.1002/jtr.2380

Termonia P, Van Schaeybroeck B, De Cruz L, De Troch R, Caluwaerts S, Giot O, Hamdi R, Vannitsem S, Duchêne F, Willems P, Tabari H, Van Uytven E, Hosseinzadehtalaei P, VanLipzig N, Wouters H, Vanden Broucke S, van Ypersele J-P, Marbaix P, Villanueva-Birriel C, Fettweis X, Wyard C, Scholzen C, Doutreloup S, De Ridder K, Gobin A, Lauwaet D, Stavrakou T, Bauwens M, Müller J-F, Luyten P, Ponsar S, Van den Eynde D, Pottiaux E., 2018. The CORDEX.be initiative as a foundation for climate services in Belgium. Climate Services 11, Pages 49-61, 2018, doi: 10.1016/j.cliser.2018.05.001.

Van de Vyver, H., Van Schaeybroeck, B., De Troch, R., De Cruz, L., Hamdi, R., Villanueva-Birriel, C., Marbaix, P., van Ypersele, J-P, Wouters, H., Vanden Broucke, S., van Lipzig, N.P.M., Doutreloup, S., Wyard, C., Scholzen, Fettweis, X., Caluwaerts, C. and Termonia, P, 2021. Evaluation framework for sub-daily rainfall extremes simulated by regional climate models, Accepted in Journal of Applied Meteorology and Climatology.

van Meijgaard E, van Ulft LH, Lenderink G, de Roode SR, Wipfler L, Boers R, Timmermans RMA (2012) Refinement and application of a regional atmospheric model for climate scenario

calculations of Western Europe. KvR 054/12, ISBN/EAN 978-90-8815-046-3, Climate changes Spatial Planning, URL https://library.wur.nl/WebQuery/wurpubs/fulltext/312258

van Oldenborgh, G.J., van der Wiel, K., Kew, S. et al. (2021). Pathways and pitfalls in extreme event attribution. *Climatic Change*, 166**,** 13, https://doi.org/10.1007/s10584-021-03071-7.

Vautard, R., van Oldenborgh, G. J., Thao, S., Dubuisson, B., Lenderink, G., Ribes, A., Planton, S., Soubeyroux, J.-M. & Yiou, P. (2015). 12. EXTREME FALL 2014 PRECIPITATION IN THE CÉVENNES MOUNTAINS. Bulletin of the American Meteorological Society, 96(12), S56-S60.

Vautard, R., Kadygrov, N., Iles, C., Boberg, F., Buonomo, E., Bülow, K., ... & Wulfmeyer, V. (2020). Evaluation of the large EURO-CORDEX regional climate model ensemble. Journal of Geophysical Research: Atmospheres, e2019JD032344. doi: https://doi.org/10.1029/2019JD032344

Wasko, C., and A. Sharma, 2015: Steeper temporal distribution of rain intensity at higher temperatures within Australian storms. Nat. Geosci., 8, 527–529, https://doi.org/10.1038/ngeo2456.

Westra, S., Alexander, L. V., & Zwiers, F. W. (2013). Global increasing trends in annual maximum daily precipitation. Journal of climate, 26(11), 3904-3918.

Zeder J., Fischer E. M. (2020): Observed extreme precipitation trends and scaling in Central Europe, Weather and Climate Extremes, Volume 29, https://doi.org/10.1016/j.wace.2020.100266.

Zier Ch. , Bäse F. , Komischke H. (2021): Ein Verfahren zur Plausibilisierung und Bewertung regionaler Klimaprojektionen. promet, Heft 104, 9-18, DOI: 10.5676/DWD_pub/promet_104_02 (German)